

Physical implications of a double right-handed gauge symmetry

Duong Van Loi,^{1,*} A. E. Cárcamo Hernández,^{2,3,4,†} N. T. Duy,^{5,‡} D. T. Binh,^{6,7,§} and Cao H. Nam^{8,9,¶}

¹*Phenikaa Institute for Advanced Study, Phenikaa University, Nguyen Trac, Duong Noi, Hanoi 100000, Vietnam*

²*Universidad Técnica Federico Santa María, Casilla 110-V, Valparaíso, Chile*

³*Centro Científico-Tecnológico de Valparaíso, Casilla 110-V, Valparaíso, Chile*

⁴*Millennium Institute for Subatomic Physics at High-Energy Frontier (SAPHIR), Fernández Concha 700, Santiago, Chile*

⁵*Institute of Physics, Vietnam Academy of Science and Technology, 10 Dao Tan, Giang Vo, Hanoi 100000, Vietnam*

⁶*Laboratory of Advanced Materials and Natural Resources,*

Institute for Advanced Study in Technology, Ton Duc Thang University, Ho Chi Minh City, Vietnam

⁷*Faculty of Applied Sciences, Ton Duc Thang University, Ho Chi Minh City, Vietnam*

⁸*Institute of Theoretical and Applied Research, Duy Tan University, Hanoi 100000, Vietnam*

⁹*School of Engineering and Technology, Duy Tan University, Da Nang 550000, Vietnam*

(Dated: January 15, 2026)

Guided by the flipping principle, we propose a novel extension of the Standard Model based on a double right-handed $U(1)$ gauge symmetry. In this framework, all left-handed fermions are neutral, while right-handed fermions of the third generation carry charges distinct from those of the first two generations. This structure naturally explains the observed Standard Model fermion mass hierarchy: the heavy masses of the third generation are generated at tree level, while the lighter masses of the first and second generations arise radiatively at the one-loop level. For the active neutrino sector, the tiny masses are generated through a combination of tree-level and two-loop seesaw mechanisms. Crucially, this approach successfully reproduces the observed neutrino mass hierarchy, with the atmospheric mass-squared difference generated at tree level and the solar neutrino mass squared difference emerging at the two-loop level. These hierarchical patterns stem from the interplay between gauge invariance and a residual parity symmetry that survives the spontaneous breaking of the extended gauge group. The same residual symmetry stabilizes a viable scalar singlet dark matter candidate, which we show can reproduce the observed relic abundance while remaining consistent with current direct detection bounds. After addressing constraints from electroweak precision tests and flavor-changing neutral currents, we explore the discovery prospects for the new neutral bosons at existing and future colliders, including the LEP, LHC, and a future ILC.

I. INTRODUCTION

Despite its remarkable successes, the Standard Model (SM) of particle physics remains incomplete, as it fails to account for several fundamental puzzles. These include the pronounced hierarchy in charged fermion masses [1], the tiny but nonzero masses and mixings of neutrinos [2, 3], and the existence of dark matter (DM) in the universe [4]. A wide range of extensions to the SM have been proposed to address these open questions. Among them, particularly compelling are those that offer a unified explanation of multiple phenomena while remaining testable at current or future experiments. In this work, we propose such a model, guided by the flipping principle.

It is well known that the matter content of the V-A theory, including left-handed fermions, transforms universally as isodoublets under the $SU(2)_L$ symmetry of weak isospin $T_{1,2,3}$ [5–7]. The electric charges of these multiplets are given by $Q = \text{diag}(0, -1)$ for $l_{aL} = (\nu_{aL}, e_{aL})^T$ and $Q = \text{diag}(2/3, -1/3)$ for $q_{aL} = (u_{aL}, d_{aL})^T$, where $a = 1, 2, 3$ denotes the generation index. Since Q neither commutes with nor closes algebraically with the weak isospin generators, i.e., $[Q, T_1 \pm iT_2] = \pm(T_1 \pm iT_2) \neq 0$ and $\text{Tr}Q \neq 0$, the $SU(2)_L$ symmetry must be extended (or flipped) to $SU(2)_L \otimes U(1)_Y$, where $Y = Q - T_3$ is identified as hypercharge. This leads to the electroweak theory, which necessarily includes right-handed fermion singlets e_{aR} , u_{aR} , and d_{aR} to ensure cancellation of $U(1)_Y$ anomalies [8, 9].

* loi.duongvan@phenikaa-uni.edu.vn (corresponding author)

† antonio.carcamo@usm.cl

‡ ntduy@iop.vast.vn

§ dinhthanhbinh@tdtu.edu.vn

¶ caohoangnam@duytan.edu.vn

By introducing a dark charge D as a generalized variant of the electric charge Q , gauge invariance and anomaly cancellation require $D = \text{diag}(\delta, \delta - 1)$ for lepton doublets l_{aL} and $D = \text{diag}(2/3 - \delta/3, -1/3 - \delta/3)$ for quark doublets q_{aL} [10–13]. For $\delta = 0$, the dark charge D reproduces the electric charge Q , while for $\delta \neq 0$ it becomes a distinct quantum number. Similar to Q , the charge D neither commutes with nor closes algebraically with the weak isospin generators. Consequently, the electroweak sector must be extended to $SU(2)_L \otimes U(1)_Y \otimes U(1)_N$, where $N = D - T_3$ is identified as the hyperdark charge. The presence of this additional Abelian symmetry necessitates three right-handed neutrinos ν_{aR} to cancel $U(1)_N$ -related anomalies. In addition, a scalar singlet with $D = -2\delta$ is required to spontaneously break $U(1)_N$ to a residual parity and to generate large Majorana masses for the right-handed neutrinos.¹

A remarkable feature of the model is that the SM Higgs doublet $H = (H^+, H^0)^T$ transforms nontrivially under the dark charge. Its components carry dark charges $D(H^+) = 1$ and $D(H^0) = 0$, ensuring that the electroweak vacuum expectation value (VEV) does not break the dark symmetry. An even more interesting phenomenon emerges at the specific value $\delta = 1/2$. At this point, the hyperdark charge undergoes a structural simplification: all left-handed fermions become automatically neutral, while all nonzero charges reside solely in the right-handed sector. This chiral reorganization has a well-defined theoretical origin. When $\delta = 1/2$, the hyperdark charge precisely matches the T_{3R} quantum number in left-right symmetric models and reproduces Abelian charge patterns arising in decompositions of the grand unified groups $SO(10)$ and E_6 . Consequently, $\delta = 1/2$ singles out a theoretically preferred Abelian extension—denoted $U(1)_R$ —that possesses a minimal and anomaly-free charge structure naturally aligned with well-motivated ultraviolet completions.

However, fermion generations remain universal under the extended gauge symmetry, as in the SM. Consequently, the observed hierarchical structure of fermion masses cannot be explained without postulating a large hierarchy among Yukawa coupling constants. This motivates us to further flip the hypercharge symmetry $U(1)_Y$ into $U(1)_Y \otimes U(1)_R$, such that only right-handed fermions of the first two generations carry nonzero $U(1)_R$ charges, while remaining fermion multiplets and the SM Higgs doublet remain neutral under $U(1)_R$, following an approach similar to that proposed in Ref. [23].

In this setup, the SM Higgs doublet provides only the tree-level mass terms for the third generation of SM charged fermions. To generate the masses of the first and second fermion families, we introduce an additional scalar doublet charged under the new gauge group $U(1)_R$, whose VEV is much smaller than that of the SM Higgs. This small VEV is arranged to vanish at tree level by a suitable choice of parameters in the scalar potential and is subsequently induced at the one-loop level after spontaneous breaking of $U(1)_Y \otimes U(1)_R$. The loop diagram responsible for this effect involves three scalar fields that are odd under a residual parity. Mechanisms for generating such a small VEV through radiative effects in multi-scalar extensions of the SM have been studied in the literature [23–26].

Furthermore, tiny masses for active neutrinos are generated from a combination of tree-level and two-loop seesaw mechanisms. Consequently, this mechanism naturally yields the observed neutrino mass hierarchy: the atmospheric mass-squared difference originates at tree level, whereas the solar neutrino mass squared difference emerges at the two-loop level. Finally, the lightest among parity-odd scalar fields running in the loop is stabilized by the residual parity, thereby providing a viable DM candidate compatible with constraints arising from DM relic abundance and DM direct detection.

The rest of this paper is organized as follows. In Sec. II, we present the structure of the model and examine mass spectra in scalar and gauge sectors. Fermion mass generation is analyzed in Sec. III. New physics (NP) phenomena and experimental constraints are discussed in Sec. IV. In Sec. V, we study the DM relic abundance and prospects for direct detection. Finally, Sec. VI is devoted to our summary and conclusions. Details of the tiny VEV for the additional Higgs doublet and the mass matrix in the scalar sector are collected in Appendices A and B, respectively.

¹ In contrast to this construction, in many existing DM models the stabilizing symmetry—typically a discrete \mathbb{Z}_2 parity—is imposed by hand at the outset, rather than emerging as a residual symmetry of a spontaneously broken gauge symmetry [14–22].

II. THE MODEL

A. Gauge symmetry, particle content, and symmetry breaking

We consider an extended $2 + 1$ Higgs doublet model where the scalar content is augmented by the inclusion of several gauge singlet scalar fields and the SM fermion sector is enlarged by the inclusion of right handed Majorana neutrinos. Our model is based on the gauge symmetry group

$$SU(3)_C \otimes SU(2)_L \otimes U(1)_Y \otimes U(1)_{\mathcal{R}} \otimes U(1)_R, \quad (1)$$

where the first two factors are exactly those of the SM gauge symmetry, while the next two arise from a decomposition of the SM hypercharge group, i.e., $U(1)_Y \rightarrow U(1)_Y \otimes U(1)_{\mathcal{R}}$. The final factor, $U(1)_R$, represents an alternative hypercharge symmetry motivated by the flipping principle, which introduces a dark charge D as a variant of the electric charge Q [10–13]. Accordingly, the electric charge and dark charge operators are defined as follows:

$$Q = T_3 + \mathcal{Y} + \mathcal{R}, \quad D = T_3 + R. \quad (2)$$

The fermion content and their charge assignments under the gauge symmetry in Eq. (1) are summarized in Table I, where the parameter z is an arbitrary nonzero constant, and ν_{aR} ($a = 1, 2$) denote new fermions introduced to ensure anomaly cancellation within each fermion generation. It is worth noting that only right-handed fermions are charged under $U(1)_R$, whereas only the right-handed fermions of the first two generations carry nonzero charges under $U(1)_{\mathcal{R}}$.

Multiplets	$SU(3)_C \otimes SU(2)_L$	$U(1)_Y$	$U(1)_{\mathcal{R}}$	$U(1)_R$	P_D
$l_{aL} = (\nu_{aL}, e_{aL})^T$	(1, 2)	-1/2	0	0	+
$\nu_{\alpha R}$	(1, 1)	-z	z	1/2	+
ν_{3R}	(1, 1)	0	0	1/2	+
$e_{\alpha R}$	(1, 1)	-1 + z	-z	-1/2	+
e_{3R}	(1, 1)	-1	0	-1/2	+
$q_{aL} = (u_{aL}, d_{aL})^T$	(3, 2)	1/6	0	0	+
$u_{\alpha R}$	(3, 1)	2/3 - z	z	1/2	+
u_{3R}	(3, 1)	2/3	0	1/2	+
$d_{\alpha R}$	(3, 1)	-1/3 + z	-z	-1/2	+
d_{3R}	(3, 1)	-1/3	0	-1/2	+

TABLE I: Fermion content of the model, where $a = 1, 2, 3$ and $\alpha = 1, 2$ are generation indices.

In addition to the fermion content listed in Table I, the model includes a scalar sector summarized in Table II. The scalar doublet Φ_1 is identified as the SM Higgs doublet, responsible for generating large masses for the third-generation of SM charged fermions: the top quark, bottom quark, and tau lepton. The neutral component of the second doublet, Φ_2 , acquires a vacuum expectation value (VEV) much smaller than the VEV of the neutral part of Φ_1 . The second scalar doublet Φ_2 is introduced to generate small masses for the first generation of SM charged fermions. The scalar singlets χ_1 and χ_3 are required to generate Majorana masses for $\nu_{\alpha R}$ and ν_{3R} , respectively. Finally, the singlets χ_2 and $\eta_{1,2}$, together with the scalar doublet ϕ , are included to induce the small VEV for Φ_2 through one-loop radiative corrections.

The remaining gauge symmetry is spontaneously broken in three stages:

$$\begin{aligned}
 & SU(2)_L \otimes U(1)_Y \otimes U(1)_{\mathcal{R}} \otimes U(1)_R \\
 & \quad \downarrow \Lambda_3 \\
 & SU(2)_L \otimes U(1)_Y \otimes U(1)_{\mathcal{R}} \otimes P_R \\
 & \quad \downarrow \Lambda_{1,2} \\
 & SU(2)_L \otimes U(1)_Y \otimes P_R \\
 & \quad \downarrow v_{1,2} \\
 & U(1)_Q \otimes P_D
 \end{aligned}$$

Multiplets	$SU(3)_C \otimes SU(2)_L$	$U(1)_Y$	$U(1)_{\mathcal{R}}$	$U(1)_{\mathcal{R}}$	P_D
$\Phi_1 = (\Phi_1^+, \Phi_1^0)^T$	(1, 2)	1/2	0	1/2	+
$\Phi_2 = (\Phi_2^+, \Phi_2^0)^T$	(1, 2)	1/2 - z	z	1/2	+
χ_1	(1, 1)	-2 z	2 z	-1	+
χ_2	(1, 1)	- $z/3$	$z/3$	0	+
χ_3	(1, 1)	0	0	-1	+
$\phi = (\phi^+, \phi^0)^T$	(1, 2)	1/2 - $z/3$	$z/3$	0	-
η_1	(1, 1)	- $z/3$	$z/3$	1/2	-
η_2	(1, 1)	0	0	1/2	-

TABLE II: Scalar content of the model.

The VEVs responsible for triggering the spontaneous breaking of the gauge symmetry are given by:

$$\langle \chi_1 \rangle = \frac{1}{\sqrt{2}} \Lambda_1, \quad \langle \chi_2 \rangle = \frac{1}{\sqrt{2}} \Lambda_2, \quad \langle \chi_3 \rangle = \frac{1}{\sqrt{2}} \Lambda_3, \quad (3)$$

$$\langle \Phi_1 \rangle = \frac{1}{\sqrt{2}} \begin{pmatrix} 0 \\ v_1 \end{pmatrix}, \quad \langle \Phi_2 \rangle = \frac{1}{\sqrt{2}} \begin{pmatrix} 0 \\ v_2 \end{pmatrix}. \quad (4)$$

These VEVs satisfy the hierarchy $\Lambda_{1,2,3} \gg v_{1,2}$, with $v_1^2 + v_2^2 = v^2 \simeq (246 \text{ GeV})^2$, to ensure consistency with the SM. In addition, we impose two further hierarchies: $\Lambda_3 \gg \Lambda_{1,2}$ to support the generation of tiny neutrino masses, and $v_2 \ll v_1$ to account for the hierarchical structure of the SM charged fermion masses. The latter is naturally realized by assuming that the VEV of Φ_2 vanishes at tree level and is generated only at one loop, after the second stage of gauge symmetry breaking, as discussed in Appendix A.

After the first stage of gauge symmetry breaking, the group $U(1)_{\mathcal{R}}$ is reduced to a residual parity $P_{\mathcal{R}} = (-1)^{2\mathcal{R}}$, as the VEV of χ_3 preserves this symmetry, i.e., $P_{\mathcal{R}}\langle \chi_3 \rangle = \langle \chi_3 \rangle$. This residual parity remains conserved through the second stage of symmetry breaking. However, in the third stage, $P_{\mathcal{R}}$ is effectively replaced by a new residual parity $P_D = (-1)^{2D}$, as a result of the VEVs of the scalar doublets $\Phi_{1,2}$. This occurs because $\mathcal{R}\langle \Phi_{1,2} \rangle = (0 \ v_{1,2}/2\sqrt{2})^T \neq 0$ and $P_D\langle \Phi_{1,2} \rangle = \langle \Phi_{1,2} \rangle$. Moreover, the singlet fields $\chi_{1,2,3}$ also preserve this new parity, satisfying $P_D\langle \chi_{1,2,3} \rangle = \langle \chi_{1,2,3} \rangle$.

It is well known that spin parity, defined as $P_s = (-1)^{2s}$, is always conserved due to Lorentz invariance. We thus define a final residual parity by combining spin parity with the dark parity as

$$P_D = (-1)^{2D+2s}, \quad (5)$$

which remains conserved in our model. This parity plays a similar role to the matter parity in supersymmetric theories [27]. The P_D assignments of all fermions and scalars are shown in the last columns of Tables I and II, respectively. All fermions, as well as the scalars $\Phi_{1,2}$ and $\chi_{1,2,3}$, are P_D -even, while the scalars ϕ and $\eta_{1,2}$ are P_D -odd. As a result, the latter fields cannot acquire VEVs.

B. Scalar sector

Given the scalar content described above, the scalar potential of our model can be decomposed into three parts, $V = V_1 + V_2 + V_3$, as presented in Appendix A. The term V_1 contains the self-interactions of the fields $\Phi_{1,2}$ and $\chi_{1,2}$. The term V_2 includes the self-interactions of ϕ and $\eta_{1,2}$, as well as their interactions with $\Phi_{1,2}$ and $\chi_{1,2}$. Finally, V_3 consists of the potential for χ_3 and its interactions with the remaining scalar fields. We assume that the parameters of the scalar potential are chosen such that the potential is bounded from below and gives rise to the desired vacuum structure. In particular, we consider a strong hierarchy $|\mu_8| \gg |\mu_{1,2,\dots,7}|$, which ensures that χ_3 effectively decouples from the low-energy spectrum. As implied by V_3 , the scalar field χ_3 acquires a large VEV, given approximately by $\Lambda_3 \simeq -\mu_8^2/\lambda_{32}$. We expand χ_3 as $\chi_3 = \frac{1}{\sqrt{2}} (\Lambda_3 + H_{\mathcal{R}} + iG_{Z_{\mathcal{R}}})$, where $H_{\mathcal{R}}$ is a heavy physical Higgs boson with mass $m_{H_{\mathcal{R}}} \simeq \sqrt{2}\Lambda_3$, and $G_{Z_{\mathcal{R}}}$ is the would-be Goldstone boson that is absorbed by the $U(1)_{\mathcal{R}}$ gauge boson.

Below the Λ_3 scale, the effective scalar potential takes the form

$$V_{\text{eff}} \simeq V_1 + V_2 + \left(\mu_0^2 \Phi_1^\dagger \Phi_2 + \text{H.c.} \right), \quad (6)$$

which generates the scalar mass matrices presented in Appendix B. Assuming the hierarchy $\Lambda_1 \sim \Lambda_2 \gg v_1 \sim \sqrt{-\mu_0^2} \gg v_2$, the mass-squared matrix M_S^2 of the P_D -even CP-even neutral scalars (S_1, S_2, S_3, S_4) can be diagonalized using the seesaw approximation, separating the light state S_1 from the heavy states S_2, S_3 , and S_4 . In the resulting physical basis $(H, \mathcal{H}, H_1, H_2)$, the mass eigenstates are approximately given by

$$H \simeq S_1 - \epsilon_1 S_2 - \epsilon_2 S_3 - \epsilon_3 S_4, \quad (7)$$

$$\mathcal{H} \simeq \epsilon_1 S_1 + S_2, \quad H_1 \simeq \epsilon_2 S_1 + S_3, \quad H_2 \simeq \epsilon_3 S_1 + S_4, \quad (8)$$

where the mixing parameters $\epsilon_{1,2,3}$ are small due to hierarchical suppression, i.e.,

$$\epsilon_1 \simeq -\frac{2\lambda_1 v_1 v_2}{\mu_0^2}, \quad \epsilon_2 \simeq \frac{\lambda_7 \lambda_8 v_1}{(\lambda_7^2 - 4\lambda_5 \lambda_6)\Lambda_2}, \quad \epsilon_3 \simeq \frac{2\lambda_5 \lambda_8 \Lambda_1 v_1}{(4\lambda_5 \lambda_6 - \lambda_7^2)\Lambda_2^2}. \quad (9)$$

The lightest state H is decoupled from the heavy sector and plays the role of the SM-like Higgs boson, with mass approximately given by

$$m_H^2 \simeq 2\lambda_1 v_1^2 - \frac{\mu_0^2 v_2}{v_1} - \epsilon_1 \mu_0^2 - \epsilon_2 \lambda_8 \Lambda_1 v_1 - \epsilon_3 \lambda_{10} \Lambda_2 v_1, \quad (10)$$

which lies at the electroweak scale. The state \mathcal{H} , with mass

$$m_{\mathcal{H}}^2 \simeq -\frac{\mu_0^2 v_1}{v_2}, \quad (11)$$

can be safely treated as a separate heavy eigenstate, since its mixing with $H_{1,2}$ is suppressed by $v_2/\Lambda_{1,2}$. The remaining scalars H_1 and H_2 mix through a 2×2 submatrix, approximately given by the bottom-right block of M_S^2 . Diagonalizing this submatrix yields two physical states, \mathcal{H}_1 and \mathcal{H}_2 , with large masses at the $\Lambda_{1,2}$ scales.

For the P_D -even CP-odd neutral scalars (A_1, A_2, A_3, A_4), we obtain two massless eigenstates,

$$G_{Z_{\mathcal{R}}} = \frac{6\Lambda_1 A_3 + \Lambda_2 A_4}{\sqrt{36\Lambda_1^2 + \Lambda_2^2}}, \quad \mathcal{G} = \frac{\Lambda_2 A_3 - 6\Lambda_1 A_4}{\sqrt{36\Lambda_1^2 + \Lambda_2^2}}, \quad (12)$$

in addition to two eigenstates arising from the M_A^2 matrix,

$$G_Z = c_\varphi A_1 + s_\varphi A_2, \quad \mathcal{A} = s_\varphi A_1 - c_\varphi A_2, \quad (13)$$

where G_Z is also massless, while \mathcal{A} is a heavy physical state with mass

$$m_{\mathcal{A}}^2 = -\frac{\mu_0^2 v^2}{v_1 v_2} = m_{\mathcal{H}}^2 \frac{v^2}{v_1^2}. \quad (14)$$

Above, we define $c_\varphi \equiv \cos \varphi = v_1/v$ and $s_\varphi \equiv \sin \varphi = v_2/v$ for brevity. The massless modes $G_{Z_{\mathcal{R}}}$ and G_Z are identified as the Goldstone bosons absorbed by the $Z_{\mathcal{R}}$ and Z gauge bosons, respectively. The state \mathcal{G} , on the other hand, remains a physical massless boson. As discussed in Ref. [28], the presence of such a massless scalar does not pose a phenomenological problem. The reason is that \mathcal{G} does not couple directly to SM particles, except for the SM-like Higgs boson H . Even in that case, the coupling strength is controlled by the potential parameters $\lambda_{8,10}$, which are required to be $|\lambda_{8,10}| \lesssim \mathcal{O}(10^{-3})$ to suppress observable effects. Furthermore, \mathcal{G} decouples from the thermal bath in the early universe at a temperature of order $\mathcal{O}(1)$ GeV, provided that all new scalar states reside at the TeV scale. Consequently, it remains consistent with standard cosmology.

Since the masslessness of \mathcal{G} originates from an accidental global symmetry, it may be lifted by Planck-suppressed operators. A gauge-invariant dimension-five operator consistent with the charge assignment in Table II is $\frac{1}{M_P} (\Phi_2^\dagger \Phi_1) \chi_2^3 + \text{H.c.}$, which explicitly breaks the accidental symmetry, where M_P denotes the Planck mass [29, 30]. For typical scales $v_1 \sim 10^2$ GeV, $v_2 \sim 1$ GeV, and $\Lambda_2 \sim 10$ TeV, this operator induces $\Delta V \sim v_1 v_2 \Lambda_2^3 / M_P$ and yields a pseudo-goldstone

mass of order $m_{\mathcal{G}} \sim 10^2$ eV. Such a mass is small enough to evade stringent bounds from tests of non-Newtonian forces [31].

For the remaining neutral scalar fields, the model contains two 3×3 mass-squared matrices, \mathcal{M}_S^2 for the CP-even states (S_5, S_6, S_7) and \mathcal{M}_A^2 for the CP-odd states (A_5, A_6, A_7) as shown in Eqs. (B9) and (B11). In both matrices, the off-diagonal elements are strongly suppressed by the hierarchy $v_2 \sim \mu \ll v_1 \ll \Lambda_{1,2}$, and are therefore much smaller than the diagonal entries. As a result, mixing effects can be safely neglected, and the fields $S_{5,6,7}$ and $A_{5,6,7}$ may be treated as approximate mass eigenstates. In this limit, each pair (S_i, A_i) ($i = 5, 6, 7$) becomes mass-degenerate and naturally combines into a physical complex scalar field,

$$\phi^0 \equiv \frac{1}{\sqrt{2}}(S_5 + iA_5), \quad \eta_1 \equiv \frac{1}{\sqrt{2}}(S_6 + iA_6), \quad \eta_2 \equiv \frac{1}{\sqrt{2}}(S_7 + iA_7), \quad (15)$$

with approximate masses

$$m_{\phi^0}^2 \simeq \mu_5^2 + \frac{1}{2}(\lambda_{20}\Lambda_1^2 + \lambda_{21}\Lambda_2^2), \quad m_{\eta_1}^2 \simeq \mu_6^2 + \frac{1}{2}(\lambda_{26}\Lambda_1^2 + \lambda_{27}\Lambda_2^2), \quad m_{\eta_2}^2 \simeq \mu_7^2 + \frac{1}{2}(\lambda_{30}\Lambda_1^2 + \lambda_{31}\Lambda_2^2). \quad (16)$$

For the charged scalar sector, the field ϕ^\pm is a physical eigenstate with a large mass given by

$$m_{\phi^\pm}^2 \simeq \mu_5^2 + \frac{1}{2}(\lambda_{20}\Lambda_1^2 + \lambda_{21}\Lambda_2^2), \quad (17)$$

which lies at the $\Lambda_{1,2}$ scale. The charged components of the Higgs doublets, Φ_1^\pm and Φ_2^\pm , mix through a 2×2 submatrix identical to the top-left block of the full charged scalar mass matrix M_C^2 . Diagonalizing this submatrix yields a massless eigenstate $G_W^\pm = c_\varphi \Phi_1^\pm + s_\varphi \Phi_2^\pm$, which is identified as the Goldstone boson absorbed by the W^\pm gauge boson, and a heavy charged scalar

$$\mathcal{H}^\pm = s_\varphi \Phi_1^\pm - c_\varphi \Phi_2^\pm, \quad (18)$$

with mass

$$m_{\mathcal{H}^\pm}^2 = -\frac{(2\mu_0^2 + \lambda_4 v_1 v_2)v^2}{2v_1 v_2} = m_{\mathcal{A}}^2 - \frac{\lambda_4}{2}v^2, \quad (19)$$

which typically lies at the TeV scale.

C. Gauge boson sector

The covariant derivative in our model is defined as

$$D_\mu = \partial_\mu + ig_s t_p G_{p\mu} + ig T_j A_{j\mu} + ig_1 \mathcal{Y} B_{1\mu} + ig_2 \mathcal{R} B_{2\mu} + ig_{\mathcal{D}} \mathcal{R} C_\mu,$$

where $(g_s, g, g_1, g_2, g_{\mathcal{D}})$ denote the gauge coupling constants, $(t_p, T_j, \mathcal{Y}, \mathcal{R}, \mathcal{C})$ are the corresponding generators, and $(G_{p\mu}, A_{j\mu}, B_{1\mu}, B_{2\mu}, C_\mu)$ are the gauge bosons associated with the groups $SU(3)_C$, $SU(2)_L$, $U(1)_Y$, $U(1)_{\mathcal{R}}$, and $U(1)_{\mathcal{D}}$, respectively. As previously mentioned, the gauge boson of the $U(1)_{\mathcal{R}}$ group, denoted by $Z_{\mathcal{R}} \equiv C_\mu$, acquires a large mass through the spontaneous breaking of the symmetry at the Λ_3 scale. Its mass is approximately given by

$$m_{Z_{\mathcal{R}}} \simeq 2g_{\mathcal{D}}\Lambda_3, \quad (20)$$

rendering it effectively decoupled from the low-energy particle spectrum. In this context, any possible kinetic mixing between C_μ and the $U(1)_Y$ and $U(1)_{\mathcal{R}}$ gauge bosons, $B_{1\mu}$ and $B_{2\mu}$, becomes irrelevant and can be safely neglected. Moreover, potential kinetic mixing between $B_{1\mu}$ and $B_{2\mu}$, if present, would induce effects that are subdominant compared to the mass mixing effects arising from spontaneous symmetry breaking. These effects are therefore suppressed, in agreement with the results of Refs. [32, 33].

Besides the heavy gauge boson $Z_{\mathcal{R}}$, the masses of the remaining gauge bosons arise from the scalar kinetic terms, $\sum_S (D^\mu S)^\dagger (D_\mu S)$, where the sum runs over all scalar fields $S = \Phi_{1,2}, \chi_{1,2}$. Since all scalar multiplets are color singlets,

the $SU(3)_C$ symmetry remains unbroken and the gluons remain massless, as expected. Defining the charged gauge bosons as

$$W_\mu^\pm \equiv \frac{1}{\sqrt{2}}(A_{1\mu} \mp iA_{2\mu}), \quad (21)$$

we obtain the mass term $\mathcal{L} \supset \frac{g^2 v^2}{4} W^\mu W_\mu$, which is identical to the SM result. The W gauge boson is a physical eigenstate by itself with mass

$$m_W^2 = \frac{g^2 v^2}{4},$$

which lies at the electroweak scale. This matches the SM prediction and allows us to identify $v \simeq 246$ GeV.

The neutral gauge bosons $A_{3\mu}$, $B_{1\mu}$, and $B_{2\mu}$ mix through the mass matrix M_0^2 ,

$$\mathcal{L} \supset \frac{1}{2}(A_3^\mu, B_1^\mu, B_2^\mu) M_0^2 (A_{3\mu}, B_{1\mu}, B_{2\mu})^T, \quad (22)$$

where

$$M_0^2 = \frac{g^2}{4} \begin{pmatrix} v^2 & \frac{g_1(2zv_2^2 - v^2)}{g} & -\frac{2g_2zv_2^2}{g} \\ \frac{g_1(2zv_2^2 - v^2)}{g} & \frac{g_1[4z^2(36\Lambda_1^2 + \Lambda_2^2) + 9v_1^2 + 9(1-2z)^2v_2^2]}{9g^2} & \frac{2g_1g_2z[9v_2^2(1-2z) - 2z(36\Lambda_1^2 + \Lambda_2^2)]}{9g^2} \\ -\frac{2g_2zv_2^2}{g} & \frac{2g_1g_2z[9v_2^2(1-2z) - 2z(36\Lambda_1^2 + \Lambda_2^2)]}{9g^2} & \frac{4g_2^2z^2(36\Lambda_1^2 + \Lambda_2^2 + 9v_2^2)}{9g^2} \end{pmatrix}. \quad (23)$$

The neutral gauge boson mass matrix M_0^2 possesses an exact zero eigenvalue, corresponding to the massless photon. To identify the physical mass eigenstates, we define the Weinberg angle θ_W and a mixing angle θ as

$$s_W \equiv \sin \theta_W = \frac{g_1 g_2}{\sqrt{g^2(g_1^2 + g_2^2) + g_1^2 g_2^2}}, \quad s_\theta \equiv \sin \theta = \frac{g_2}{\sqrt{g_1^2 + g_2^2}} = \frac{g_Y}{g_1},$$

where g_Y is the effective hypercharge coupling constant. Using these definitions, the gauge boson eigenstates can be expressed as orthonormal linear combinations of the original fields $A_{3\mu}$, $B_{1\mu}$, and $B_{2\mu}$:

$$A_\mu = s_W A_{3\mu} + c_W(s_\theta B_{1\mu} + c_\theta B_{2\mu}), \quad (24)$$

$$Z_\mu = c_W A_{3\mu} - s_W(s_\theta B_{1\mu} + c_\theta B_{2\mu}), \quad (25)$$

$$Z'_\mu = c_\theta B_{1\mu} - s_\theta B_{2\mu}, \quad (26)$$

where $c_W \equiv \cos \theta_W$ and $c_\theta \equiv \cos \theta$. A_μ is the photon field, Z_μ is identified with the SM Z boson, and Z'_μ is a new heavy neutral gauge boson that is orthogonal to both A_μ and Z_μ .

In the basis (A_μ, Z_μ, Z'_μ) , the photon field A_μ remains massless and fully decoupled, as expected. However, the neutral gauge bosons Z_μ and Z'_μ mix through a 2×2 submatrix of the full mass matrix. The relevant entries of this submatrix are given by

$$m_Z^2 = \frac{g^2 v^2}{4c_W^2}, \quad m_{ZZ'}^2 = \frac{g^2 v^2 [4z s_\varphi^2 - 1 - c_{2\theta}]) t_W}{4c_W s_{2\theta}}, \quad (27)$$

$$m_{Z'}^2 = \frac{g^2 \{9v^2[3 - 4(1-2z)(2z - c_{2\theta}) + c_{4\theta} + 8z(1-2z + c_{2\theta})c_{2\varphi}] + 32z^2(36\Lambda_1^2 + \Lambda_2^2)\} t_W^2}{72s_{2\theta}^2}. \quad (28)$$

Diagonalizing this submatrix yields two physical neutral gauge bosons,

$$Z_{1\mu} = c_\varepsilon Z_\mu - s_\varepsilon Z'_\mu, \quad Z_{2\mu} = s_\varepsilon Z_\mu + c_\varepsilon Z'_\mu, \quad (29)$$

with the corresponding masses approximately given by

$$m_{Z_1}^2 \simeq m_Z^2 - \frac{m_{ZZ'}^2}{m_{Z'}^2}, \quad m_{Z_2}^2 \simeq m_{Z'}^2, \quad (30)$$

under the assumption $v \ll \Lambda_{1,2}$, which ensures that Z_1 closely resembles the SM Z boson. The mixing angle ε between Z and Z' is also small and approximately given by

$$t_{2\varepsilon} \simeq -\frac{9v^2 c_\theta^3 s_\theta}{2s_W z^2 (36\Lambda_1^2 + \Lambda_2^2)}, \quad (31)$$

which confirms that the mixing is suppressed by the ratio $v^2/\Lambda_{1,2}^2$. As a result, Z_1 can be safely identified as the observed SM-like Z boson, while Z_2 is a heavy neutral gauge boson with mass at the $\mathcal{O}(\Lambda_{1,2})$ scale.

D. Fermion-gauge boson interactions

This subsection presents the interactions between fermions and gauge bosons, which originate from the kinetic term of fermion fields: $\mathcal{L}_{\text{kin}} \supset \sum_F \bar{F} i\gamma^\mu D_\mu F$, where the sum runs over all fermion multiplets in the model. The covariant derivative is rewritten in terms of physical gauge bosons as

$$\begin{aligned} D_\mu = & \partial_\mu + ig_s t_p G_{p\mu} + ig_s W Q A_\mu + ig(T_+ W_\mu^+ + \text{H.c.}) \\ & + \frac{ig}{c_W} \left[c_\varepsilon (T_3 - s_W^2 Q) + s_\varepsilon \frac{s_W}{s_\theta c_\theta} (\mathcal{R} - c_\theta^2 Y) \right] Z_{1\mu} \\ & + \frac{ig}{c_W} \left[s_\varepsilon (T_3 - s_W^2 Q) - c_\varepsilon \frac{s_W}{s_\theta c_\theta} (\mathcal{R} - c_\theta^2 Y) \right] Z_{2\mu} + ig_D \mathcal{R} Z_{R\mu}, \end{aligned} \quad (32)$$

where $T_\pm = (T_1 \pm iT_2)/\sqrt{2}$ are the weight-raising and lowering operators of the $SU(2)_L$ group. From Eq. (32), it is clear that the interactions of fermions with gluons, the photon, and the W^\pm bosons remain unchanged compared to the SM:

$$\mathcal{L} \supset -\frac{g_s}{2} \bar{q} \gamma^\mu \lambda_p q G_{p\mu} - e Q(f') \bar{f}' \gamma^\mu f' A_\mu - \frac{g}{\sqrt{2}} [(\bar{\nu}_{aL} \gamma^\mu e_{aL} + \bar{u}_{aL} \gamma^\mu d_{aL}) W_\mu^+ + \text{H.c.}], \quad (33)$$

where λ_p ($p = 1, \dots, 8$) are the Gell-Mann matrices. The fields q and f' denote quarks and charged fermions in mass eigenstate basis respectively, while ν_{aL} , e_{aL} , u_{aL} , and d_{aL} (with $a = 1, 2, 3$) represent the fermion components in the gauge eigenbasis.

The interactions between the neutral gauge bosons $Z_{1,2}$ and fermions can be written in the following form:

$$\mathcal{L} \supset -\frac{g}{2c_W} \left[C_L^{Z_I} \bar{\nu}_{aL} \gamma^\mu \nu_{aL} + C_R^{Z_I} \bar{\nu}_{\alpha R} \gamma^\mu \nu_{\alpha R} + \bar{f} \gamma^\mu \left(g_V^{Z_I}(f) - g_A^{Z_I}(f) \gamma_5 \right) f \right] Z_{I\mu}, \quad (34)$$

where $I = 1, 2$, while ν_{aL} , $\nu_{\alpha R}$, and f denote the left-handed neutrinos, right-handed neutrinos, and charged fermions in the gauge basis, respectively. Additionally, $a = 1, 2, 3$ and $\alpha = 1, 2$ are the family indices as previously defined. The coupling coefficients $C_{L,R}^{Z_I}$ and $g_{V,A}^{Z_I}(f)$ are given by the following expressions:

$$C_L^{Z_1} = c_\varepsilon + s_\varepsilon \frac{s_W}{t_\theta}, \quad C_R^{Z_1} = s_\varepsilon \frac{2z s_W}{s_\theta c_\theta}, \quad (35)$$

$$g_V^{Z_1}(f) = c_\varepsilon (T_3(f_L) - 2Q(f) s_W^2) + s_\varepsilon \frac{s_W}{s_\theta c_\theta} [\mathcal{R}(f_L) + \mathcal{R}(f_R) - c_\theta^2 (Y(f_L) + Y(f_R))], \quad (36)$$

$$g_A^{Z_1}(f) = c_\varepsilon T_3(f_L) + s_\varepsilon \frac{s_W}{s_\theta c_\theta} [\mathcal{R}(f_L) - \mathcal{R}(f_R) - c_\theta^2 (Y(f_L) - Y(f_R))], \quad (37)$$

$$C_{L,R}^{Z_2} = C_{L,R}^{Z_1}|_{c_\varepsilon \rightarrow s_\varepsilon, s_\varepsilon \rightarrow -c_\varepsilon}, \quad g_{V,A}^{Z_2}(f) = g_{V,A}^{Z_1}(f)|_{c_\varepsilon \rightarrow s_\varepsilon, s_\varepsilon \rightarrow -c_\varepsilon}. \quad (38)$$

For completeness, we present the vector and axial-vector couplings of the Z_1 (Z_2) boson to the charged fermions in Table III (Table IV). It is evident that the couplings of the Z_1 boson to the SM fermions reduce to those of the SM Z boson in the limit $\varepsilon \rightarrow 0$.

f	$g_V^{Z_1}(f)$	$g_A^{Z_1}(f)$
e_α	$c_\varepsilon (2s_W^2 - \frac{1}{2}) + s_\varepsilon s_W \left(\frac{3}{2t_\theta} - \frac{z}{s_\theta c_\theta} \right)$	$-\frac{1}{2}c_\varepsilon - s_\varepsilon s_W \left(\frac{1}{2t_\theta} - \frac{z}{s_\theta c_\theta} \right)$
e_3	$c_\varepsilon (2s_W^2 - \frac{1}{2}) + s_\varepsilon \frac{3s_W}{2t_\theta}$	$-\frac{1}{2}c_\varepsilon - s_\varepsilon \frac{s_W}{2t_\theta}$
u_α	$c_\varepsilon (\frac{1}{2} - \frac{4}{3}s_W^2) - s_\varepsilon s_W \left(\frac{5}{6t_\theta} - \frac{z}{s_\theta c_\theta} \right)$	$\frac{1}{2}c_\varepsilon + s_\varepsilon s_W \left(\frac{1}{2t_\theta} - \frac{z}{s_\theta c_\theta} \right)$
u_3	$c_\varepsilon (\frac{1}{2} - \frac{4}{3}s_W^2) - s_\varepsilon \frac{5s_W}{6t_\theta}$	$\frac{1}{2}c_\varepsilon + s_\varepsilon \frac{s_W}{2t_\theta}$
d_α	$c_\varepsilon (\frac{2}{3}s_W^2 - \frac{1}{2}) + s_\varepsilon s_W \left(\frac{1}{6t_\theta} - \frac{z}{s_\theta c_\theta} \right)$	$-\frac{1}{2}c_\varepsilon - s_\varepsilon s_W \left(\frac{1}{2t_\theta} - \frac{z}{s_\theta c_\theta} \right)$
d_3	$c_\varepsilon (\frac{2}{3}s_W^2 - \frac{1}{2}) + s_\varepsilon \frac{s_W}{6t_\theta}$	$-\frac{1}{2}c_\varepsilon - s_\varepsilon \frac{s_W}{2t_\theta}$

TABLE III: Vector and axial-vector couplings of the Z_1 boson to charged fermions.

f	$g_V^{Z^2}(f)$	$g_A^{Z^2}(f)$
e_α	$s_\varepsilon (2s_W^2 - \frac{1}{2}) - c_\varepsilon s_W \left(\frac{3}{2t_\theta} - \frac{z}{s_\theta c_\theta} \right)$	$-\frac{1}{2}s_\varepsilon + c_\varepsilon s_W \left(\frac{1}{2t_\theta} - \frac{z}{s_\theta c_\theta} \right)$
e_3	$s_\varepsilon (2s_W^2 - \frac{1}{2}) - c_\varepsilon \frac{3s_W}{2t_\theta}$	$-\frac{1}{2}s_\varepsilon + c_\varepsilon \frac{s_W}{2t_\theta}$
u_α	$s_\varepsilon \left(\frac{1}{2} - \frac{4}{3}s_W^2 \right) + c_\varepsilon s_W \left(\frac{5}{6t_\theta} - \frac{z}{s_\theta c_\theta} \right)$	$\frac{1}{2}s_\varepsilon - c_\varepsilon s_W \left(\frac{1}{2t_\theta} - \frac{z}{s_\theta c_\theta} \right)$
u_3	$s_\varepsilon \left(\frac{1}{2} - \frac{4}{3}s_W^2 \right) + c_\varepsilon \frac{5s_W}{6t_\theta}$	$\frac{1}{2}s_\varepsilon - c_\varepsilon \frac{s_W}{2t_\theta}$
d_α	$s_\varepsilon \left(\frac{2}{3}s_W^2 - \frac{1}{2} \right) - c_\varepsilon s_W \left(\frac{1}{6t_\theta} - \frac{z}{s_\theta c_\theta} \right)$	$-\frac{1}{2}s_\varepsilon + c_\varepsilon s_W \left(\frac{1}{2t_\theta} - \frac{z}{s_\theta c_\theta} \right)$
d_3	$s_\varepsilon \left(\frac{2}{3}s_W^2 - \frac{1}{2} \right) - c_\varepsilon \frac{s_W}{6t_\theta}$	$-\frac{1}{2}s_\varepsilon + c_\varepsilon \frac{s_W}{2t_\theta}$

TABLE IV: Vector and axial-vector couplings of the Z_2 boson to charged fermions.

It is noteworthy that the charges Q , T_3 , Y , and R are universal across all flavors of neutrinos, charged leptons, up-type quarks, and down-type quarks, whereas the charge \mathcal{R} is flavor-dependent. As a consequence, both Z_1 and Z_2 can mediate flavor-changing interactions among fermions. The flavor violation induced by Z_1 originates from the Z – Z' mixing and is therefore strongly suppressed. In contrast, the flavor-changing effects mediated by Z_2 can be sizable, even when $\varepsilon = 0$. In the following analysis, we focus on the flavor-changing effects arising from Z_2 and disregard those due to Z_1 , given that $|\varepsilon| \lesssim 10^{-3}$.

III. FERMION MASS AND MIXING

With the particle content and symmetries specified in Tables I and II, the following renormalizable Yukawa interactions arise

$$\begin{aligned} \mathcal{L}_{\text{Yuk}} = & h_{a\alpha}^\nu \bar{l}_{aL} i\sigma_2 \Phi_2^* \nu_{\alpha R} + h_{a\alpha}^e \bar{l}_{aL} \Phi_2 e_{\alpha R} + h_{a3}^\nu \bar{l}_{aL} i\sigma_2 \Phi_1^* \nu_{3R} + h_{a3}^e \bar{l}_{aL} \Phi_1 e_{3R} \\ & + h_{a\alpha}^u \bar{q}_{aL} i\sigma_2 \Phi_2^* u_{\alpha R} + h_{a\alpha}^d \bar{q}_{aL} \Phi_2 d_{\alpha R} + h_{a3}^u \bar{q}_{aL} i\sigma_2 \Phi_1^* u_{3R} + h_{a3}^d \bar{q}_{aL} \Phi_1 d_{3R} \\ & + \frac{1}{2} f_{\alpha\beta}^\nu \bar{\nu}_{\alpha R}^c \chi_1 \nu_{\beta R} + \frac{1}{2} f_{33}^\nu \bar{\nu}_{3R}^c \chi_3 \nu_{3R} + \text{H.c.}, \end{aligned} \quad (39)$$

where σ_2 is the second Pauli matrix, and all Yukawa couplings h 's and f 's are dimensionless. After the scalar fields acquire their VEVs at both tree and one-loop levels, the above interactions generate mass matrices for up-type quarks, down-type quarks, and charged leptons, all sharing the same texture:

$$M = -\frac{1}{\sqrt{2}} \begin{pmatrix} h_{11}v_2 & h_{12}v_2 & h_{13}v_1 \\ h_{21}v_2 & h_{22}v_2 & h_{23}v_1 \\ h_{31}v_2 & h_{32}v_2 & h_{33}v_1 \end{pmatrix}, \quad (40)$$

where the superscripts on the Yukawa couplings are omitted for brevity and should be understood from the context. This mass generation mechanism for charged fermions is illustrated by the diagrams in the first row of Fig. 1.

To derive the physical masses of charged fermions and the Cabibbo–Kobayashi–Maskawa (CKM) matrix, we decompose the Hermitian product $MM^\dagger \equiv \mathcal{M}$ into two parts: $\mathcal{M} = \mathcal{M}^{\text{tree}} + \mathcal{M}^{\text{loop}}$, where $\mathcal{M}^{\text{tree}}$ and $\mathcal{M}^{\text{loop}}$ contain terms proportional to v_1^2 and v_2^2 , respectively. Given that $v_1 \gg v_2$, the leading contributions of \mathcal{M} arise from $\mathcal{M}^{\text{tree}}$, yielding

$$\mathcal{V}_L^\dagger \mathcal{M}^{\text{tree}} \mathcal{V}_L = \text{diag} \left(0, 0, \frac{1}{2} (h_{13}^2 + h_{23}^2 + h_{33}^2) v_1^2 \right), \quad (41)$$

which corresponds to the masses of the third-family charged fermions, i.e.,

$$m_3^2 = \frac{1}{2} (h_{13}^2 + h_{23}^2 + h_{33}^2) v_1^2. \quad (42)$$

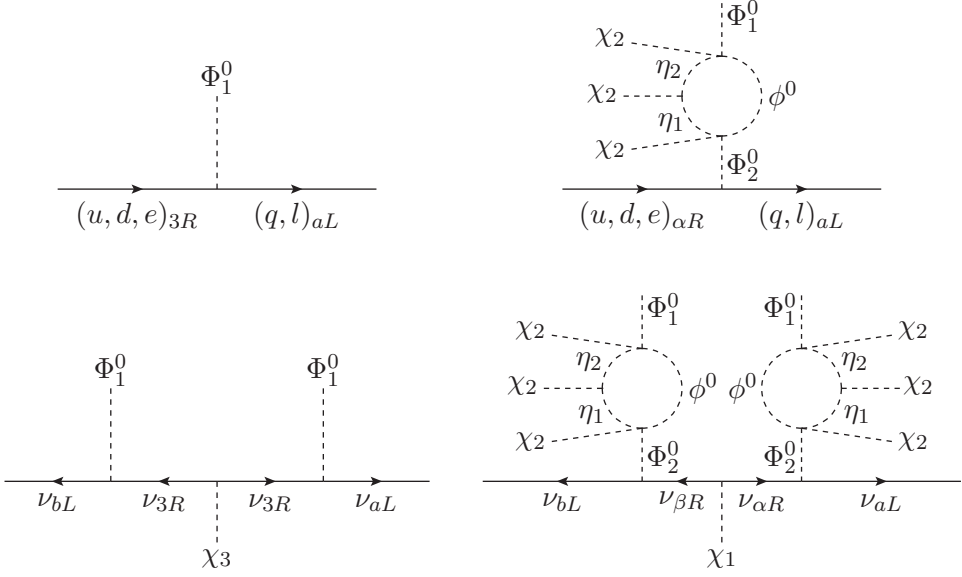


FIG. 1: Feynman diagrams contributing to the entries of the mass matrices for SM charged fermions (first row) and light active neutrinos (second row). Here $a, b = 1, 2, 3$ and $\alpha, \beta = 1, 2$.

The unitary matrix \mathcal{V}_L takes the form

$$\mathcal{V}_L = \begin{pmatrix} \frac{1}{\sqrt{2+(t_{13}+t_{23})^2}} & \frac{1+t_{23}(t_{13}+t_{23})}{\sqrt{[2+(t_{13}+t_{23})^2](1+t_{13}^2+t_{23}^2)}} & \frac{t_{13}}{\sqrt{1+t_{13}^2+t_{23}^2}} \\ \frac{1}{\sqrt{2+(t_{13}+t_{23})^2}} & -\frac{1+t_{13}(t_{13}+t_{23})}{\sqrt{[2+(t_{13}+t_{23})^2](1+t_{13}^2+t_{23}^2)}} & \frac{t_{23}}{\sqrt{1+t_{13}^2+t_{23}^2}} \\ -\frac{t_{13}+t_{23}}{\sqrt{2+(t_{13}+t_{23})^2}} & \frac{t_{23}-t_{13}}{\sqrt{[2+(t_{13}+t_{23})^2](1+t_{13}^2+t_{23}^2)}} & \frac{1}{\sqrt{1+t_{13}^2+t_{23}^2}} \end{pmatrix}, \quad (43)$$

where we have conveniently denoted $t_{13} = h_{13}/h_{33}$ and $t_{23} = h_{23}/h_{33}$.

To find the next-to-leading-order contributions of \mathcal{M} , we transform it to a new basis via the rotation $\mathcal{M}' = \mathcal{V}_L^\dagger \mathcal{M} \mathcal{V}_L$. In this rotated basis, the resulting matrix \mathcal{M}' features a dominant 3×3 element proportional to v_1^2 , while all remaining entries are suppressed by v_2^2 . This hierarchical structure allows us to apply the seesaw approximation to isolate the light (upper-left) block of \mathcal{M}' , defined as

$$\delta m^2 \equiv \begin{pmatrix} \delta m_{11}^2 & \delta m_{12}^2 \\ \delta m_{21}^2 & \delta m_{22}^2 \end{pmatrix} = \begin{pmatrix} (\mathcal{V}_L^\dagger)_{1i}(\mathcal{M})_{ij}(\mathcal{V}_L)_{j1} & (\mathcal{V}_L^\dagger)_{1i}(\mathcal{M})_{ij}(\mathcal{V}_L)_{j2} \\ (\mathcal{V}_L^\dagger)_{2i}(\mathcal{M})_{ij}(\mathcal{V}_L)_{j1} & (\mathcal{V}_L^\dagger)_{2i}(\mathcal{M})_{ij}(\mathcal{V}_L)_{j2} \end{pmatrix}, \quad (44)$$

for $i, j = 1, 2, 3$. Neglecting the seesaw-induced mixing, which is suppressed by the ratio v_2^2/v_1^2 , the submatrix δm^2 yields two nonzero eigenvalues corresponding to the physical masses of the charged fermions in the first and second families,

$$m_{1,2}^2 = \frac{1}{2} \left[\delta m_{11}^2 + \delta m_{22}^2 \mp \sqrt{(\delta m_{11}^2 - \delta m_{22}^2)^2 + 4\delta m_{21}^4} \right], \quad (45)$$

which are proportional to v_2^2 , and a rotation angle ξ to be

$$t_{2\xi} = \frac{2\delta m_{21}^2}{\delta m_{22}^2 - \delta m_{11}^2}. \quad (46)$$

Hence, the gauge eigenstates and mass eigenstates are related through the matrix $V_L = \mathcal{V}_L \mathcal{V}_\xi$, where $\mathcal{V}_\xi = \{\{c_\xi, s_\xi, 0\}, \{-s_\xi, c_\xi, 0\}, \{0, 0, 1\}\}$. For each sector of the charged fermions, the transformation is explicitly given by

$$(u_1 \ u_2 \ u_3)_L^T = V_{uL} (u \ c \ t)_L^T, \quad (d_1 \ d_2 \ d_3)_L^T = V_{dL} (d \ s \ b)_L^T, \quad (e_1 \ e_2 \ e_3)_L^T = V_{eL} (e \ \mu \ \tau)_L^T, \quad (47)$$

where the superscripts on V correspond to those on the Yukawa couplings. The CKM matrix is then defined by $V_{\text{CKM}} = V_{uL}^\dagger V_{dL}$.

Concerning the neutral leptons, the neutrinos ν_{aL} and ν_{aR} acquire a Dirac mass matrix M_D , which has the same structure as the matrix M in Eq. (40), but with the Yukawa couplings h_{ab}^ν . In addition, the right-handed neutrinos ν_{aR} receive a Majorana mass matrix of the form

$$M_M = -\frac{1}{\sqrt{2}} \begin{pmatrix} f_{11}^\nu \Lambda_1 & f_{12}^\nu \Lambda_1 & 0 \\ f_{21}^\nu \Lambda_1 & f_{22}^\nu \Lambda_1 & 0 \\ 0 & 0 & f_{33}^\nu \Lambda_3 \end{pmatrix}. \quad (48)$$

The corresponding Feynman diagrams are shown in the second row of Fig. 1. Since $\Lambda_{1,3} \gg v_{1,2}$, the canonical seesaw mechanism is naturally implemented, leading to tiny masses for the active neutrinos. These masses are generated both at tree level and through two-loop radiative corrections.

At tree level, the Dirac mass matrix receives contributions solely from v_1 . Consequently, the seesaw mechanism yields a light active neutrino mass matrix of the form

$$(m_\nu^{\text{tree}})_{ab} = \frac{h_{a3}^\nu h_{3b}^\nu}{f_{33}^\nu} \frac{v_1^2}{\sqrt{2} \Lambda_3}, \quad (49)$$

which is of rank 1. This implies that only one neutrino acquires mass at tree level, which is incompatible with experimental observations [1]. At loop level, the Dirac mass matrix is generated from v_2 , while v_1 is absent. The corresponding radiative seesaw contribution to the neutrino mass matrix becomes

$$(m_\nu^{\text{loop}})_{ab} = - (M_D M_M^{-1} M_D^T)_{ab} |_{v_1 \rightarrow 0} \sim \frac{(h_{a\alpha}^\nu)^2}{f_{\alpha\beta}^\nu} \frac{v_2^2}{\Lambda_1}. \quad (50)$$

This loop-induced mass matrix has rank 2, thereby generating masses for two additional neutrinos and bringing the model into agreement with experimental data [1]. Assuming representative parameter values such as $v_1 \sim 10^2$ GeV, $v_2 \sim 1$ GeV, $h_{ab}^\nu \sim 10^{-3}$, and $f_{\alpha\beta,33}^\nu \sim 1$, the observed neutrino mass scale $m_\nu \sim 0.1$ eV implies that $\Lambda_1 \sim 10$ TeV and $\Lambda_3 \sim 10^6$ TeV. In an alternative scenario where $h_{ab}^\nu \sim f_{33}^\nu \sim 1$, reproducing the correct neutrino mass scale would require significantly higher values for the symmetry-breaking scales, namely $\Lambda_1 \sim 10^7$ TeV and $\Lambda_3 \sim 10^{11}$ TeV.

The total neutrino mass matrix is given by

$$(m_\nu)_{ab} = (m_\nu^{\text{tree}})_{ab} + (m_\nu^{\text{loop}})_{ab}, \quad (51)$$

which has full rank (rank 3) and thus yields three non-zero neutrino masses, in agreement with experimental observations [1]. Specifically, the mass eigenvalues $m_{1,2,3}$ are obtained through the diagonalization

$$(V_L^\nu)^T m_\nu V_L^\nu = \text{diag}(m_{\nu_e}, m_{\nu_\mu}, m_{\nu_\tau}), \quad (52)$$

where V_L^ν is a unitary matrix that relates the flavor (physical) neutrino states $\nu'_L = (\nu_{eL} \nu_{\mu L} \nu_{\tau L})^T$ to the gauge eigenstates $\nu_L = (\nu_{1L} \nu_{2L} \nu_{3L})^T$ via $\nu_L = V_L \nu'_L$. Accordingly, the Pontecorvo-Maki-Nakagawa-Sakata (PMNS) matrix is defined as $U_{\text{PMNS}} = V_{\nu L}^\dagger V_{eL}$. It is worth emphasizing that the model naturally reproduces the observed neutrino mass hierarchy, with the atmospheric and solar neutrino mass-squared differences arising at tree and two-loop levels, respectively. This hierarchical pattern is a direct consequence of the separation between the effective scales Λ_1 and Λ_3 , associated with the atmospheric and solar sectors, together with the flavor structure of the corresponding Yukawa couplings. Finally, the model predicts two heavy neutrino states, which are combinations of the right-handed neutrinos $\nu_{\alpha R}$, with masses at the scale Λ_1 , and an additional very heavy neutrino, predominantly $\sim \nu_{3R}$, with a mass at the scale Λ_3 .

As summarized in Table V, the model under consideration successfully reproduces the observed masses of the SM charged fermions, the neutrino mass-squared differences, the mixing parameters and the CP phases.

The eigenvalue problem associated with the mass matrices for SM charged fermions and light active neutrinos is solved, determining a parameter set consistent with the experimental values of the physical observables of the quark and lepton sectors. One of the benchmark solutions corresponds to $v_2 \simeq 0.52$ GeV, $\Lambda_1 = 10$ TeV, and $\Lambda_3 = 10^6$ TeV,

Observable	Experimental value	Model value	Observable	Experimental value	Model value
m_u [MeV]	1.24(22)	1.2428	m_e [MeV]	0.4883266(17)	0.488327
m_c [GeV]	0.62(2)	0.619993	m_μ [MeV]	102.87267(21)	102.866
m_t [GeV]	172.9(4)	172.899	m_τ [MeV]	1747.43(12)	1747.43
m_d [MeV]	2.69(19)	2.69183	Δm_{21}^2 [10^{-5} eV 2]	7.49(19)	7.49003
m_s [MeV]	53.5(4.6)	53.3857	Δm_{31}^2 [10^{-3} eV 2]	$2.513^{+0.021}_{-0.019}$	2.513
m_b [GeV]	2.86(3)	2.86008	$\sin^2 \theta_{12}^{(l)}/10^{-1}$	$3.08^{+0.12}_{-0.11}$	3.07999
$\sin \theta_{12}^{(q)}/10^{-1}$	2.2501(68)	2.2501	$\sin^2 \theta_{23}^{(l)}/10^{-1}$	$4.70^{+0.17}_{-0.13}$	4.70076
$\sin \theta_{23}^{(q)}/10^{-2}$	$4.183^{+0.079}_{-0.069}$	4.18315	$\sin^2 \theta_{13}^{(l)}/10^{-2}$	$2.215^{+0.056}_{-0.058}$	2.215
$\sin \theta_{13}^{(q)}/10^{-3}$	$3.732^{+0.090}_{-0.085}$	3.73191	$\delta_{\text{CP}}^{(l)}$ [°]	212^{+26}_{-41}	211.926
$J_q/10^{-5}$	$3.12^{+0.13}_{-0.12}$	3.11966			

TABLE V: Experimental values of the SM charged fermion masses, neutrino mass-squared differences, and mixing parameters [1, 34, 35], along with the corresponding model predictions obtained from the best-fit solution.

and employs the following structures for the fermion mass matrices:

$$M_u \simeq \begin{pmatrix} -0.199985 + 0.15933i & -0.0155587 - 0.162743i & 3.41237 - 1.2098i \\ -0.357103 + 0.282796i & -0.0295511 - 0.29138i & 7.91538 - 1.30834i \\ (1.231 - 0.089i) \times 10^{-6} & (1.180 + 0.678i) \times 10^{-6} & 168.889 - 35.964i \end{pmatrix} \text{GeV}, \quad (53)$$

$$M_d \simeq \begin{pmatrix} 0.00920894 & 0.0347929 & 0.0043808 \\ 0.00621922 & 0.0392079 & 0.0259326 \\ 0.0010463 & 0.0166569 & 2.85991 \end{pmatrix} \text{GeV}, \quad (54)$$

$$M_e \simeq \begin{pmatrix} 0.259686 & -0.4745 & 0.000693803 \\ 102.704 & 5.77402 & 0.000513704 \\ 0.000750844 & 0.00164944 & 1747.43 \end{pmatrix} \text{MeV}, \quad (55)$$

$$m_\nu \simeq \begin{pmatrix} 3.83781 + 0.984023i & -1.40753 - 2.86153i & -6.59195 - 3.03522i \\ -1.40753 - 2.86153i & 26.8893 - 0.296409i & 21.3523 - 0.0438046i \\ -6.59195 - 3.03522i & 21.3523 - 0.0438046i & 28.548 + 0.241133i \end{pmatrix} \text{meV}. \quad (56)$$

IV. CONSTRAINTS

A. Electroweak precision test

As discussed in subsection II B, the model predicts a tree-level mixing between the SM Z boson and a new neutral gauge boson Z' . This mixing leads to a reduction in the physical mass of the Z boson compared to its SM prediction, as shown in Eq. (30). Given the precise experimental measurement of the Z -boson mass, $m_Z = 91.1880 \pm 0.0020$ GeV [1], we impose the constraint $|\Delta m_Z| < 0.0020$ GeV to maintain consistency with observations.

While the Z - Z' mixing reduces the physical mass of the SM Z boson, the mass of the W boson remains unchanged. As a result, the parameter $\rho \equiv m_W^2/(c_W^2 m_Z^2)$, which is equal to unity at tree level in the SM, receives a deviation due to the NP contributions arising from the Z - Z' mixing. This deviation can be estimated as

$$\Delta\rho = \frac{m_W^2}{c_W^2 m_{Z_1}^2} - 1 \simeq \frac{m_{ZZ'}^4}{m_Z^2 m_{Z'}^2}, \quad (57)$$

where m_{Z_1} is the mass of the lightest neutral gauge boson (identified with the observed SM Z neutral gauge boson), and $m_{ZZ'}$ denotes the off-diagonal mass term arising from the mixing. Based on the global fit to the ρ parameter, $\rho = 1.00031 \pm 0.00019$ [1], we adopt a conservative upper bound of $\Delta\rho < 0.00050$ to ensure compatibility with electroweak precision constraints.

The Z - Z' mixing also modifies the well-measured vector and axial-vector couplings of the SM Z boson to fermions, which are given by $g_V^Z(f) = T_3(f) - 2Q(f)s_W^2$ and $g_A^Z(f) = T_3(f)$. As a result of the mixing, these couplings are shifted according to

$$g_{V,A}^{Z_1}(f) = g_{V,A}^Z(f) + \mathcal{O}(\varepsilon), \quad (58)$$

where ε being the Z - Z' mixing parameter. Electroweak precision data place stringent limits on deviations from the SM predictions, allowing NP effects only if $|\varepsilon| \lesssim 10^{-3}$ [36, 37]. This requirement therefore imposes an additional constraint on the viable model parameter space.

Another constraint can be derived from the precision measurement of the total decay width of the observed Z_1 boson. Experimentally, the width is measured as $\Gamma_{Z_1}^{\text{exp}} = 2.4955 \pm 0.0023$ GeV, while the SM predicts $\Gamma_{Z_1}^{\text{SM}} = 2.4942 \pm 0.0008$ GeV [1]. To remain consistent with observation, we require the shift in decay width to satisfy $|\Delta\Gamma_{Z_1}| < 0.0044$ GeV. In our model, the shift in decay width of Z_1 can be approximately calculated as [38]

$$\begin{aligned} \Delta\Gamma_{Z_1} \simeq & \frac{m_Z}{6\pi} \left(\frac{g}{2c_W} \right)^2 \left\{ \sum_f N_C^f \left[\left| G_V^{Z_1}(f) \right|^2 \text{Re}[\delta_V^f] + \left| G_A^{Z_1}(f) \right|^2 \text{Re}[\delta_A^f] \right] + 2 \sum_i \left| G_L^{Z_1}(\nu_{iL}) \right|^2 \text{Re}[\delta^{\nu_{iL}}] \right\} \\ & + \frac{\Delta m_Z}{12\pi} \left(\frac{g}{2c_W} \right)^2 \left\{ \sum_f N_C^f \left[\left| G_V^{Z_1}(f) \right|^2 + \left| G_A^{Z_1}(f) \right|^2 \right] + 2 \sum_i \left| G_L^{Z_1}(\nu_{iL}) \right|^2 \right\}, \end{aligned} \quad (59)$$

where N_C^f is the number of color degrees of freedom for the charged fermion f , and $G_{V,A}^{Z_1}(f)$, $\delta_{V,A}^f$ denote vector and axial-vector couplings of Z_1 to f in the mass basis and their respective fractional shifts. Similarly, $G_L^{Z_1}(\nu_{iL})$ and $\delta^{\nu_{iL}}$ refer to the couplings of Z_1 to the physical neutrinos and their corresponding shifts [38].

In Fig. 2, we illustrate the correlation between the coupling g_1 of the new $U(1)_Y$ group and the NP scale Λ_1 (left panel), as well as the mass of the new gauge boson m_{Z_2} (right panel). In this analysis, we fix $z = 1$ and $v_2 \simeq 0.52$ GeV, and assume $\Lambda_1 \simeq \Lambda_2$ for simplicity. The relation $g_2 = g_1 g_Y / \sqrt{g_1^2 - g_Y^2}$ is also employed. The constraint from the Z -boson mass shift Δm_Z is substantially stronger than those arising from the ρ -parameter, the mixing parameter ε , and the decay width shift $\Delta\Gamma_{Z_1}$. Furthermore, under the gauge coupling unification condition $g_1 = g_2 = \sqrt{2}g_Y$, represented by the dashed blue line, the model predicts lower bounds of $\Lambda_1 \gtrsim 4.7$ TeV and $m_{Z_2} \gtrsim 6.9$ TeV. We emphasize that these results remain stable under variations of the parameters z and v_2 within reasonable ranges, specifically $0.01 \lesssim |z| \lesssim 20$ and $0.05 \text{ GeV} \lesssim v_2 \lesssim 10 \text{ GeV}$.

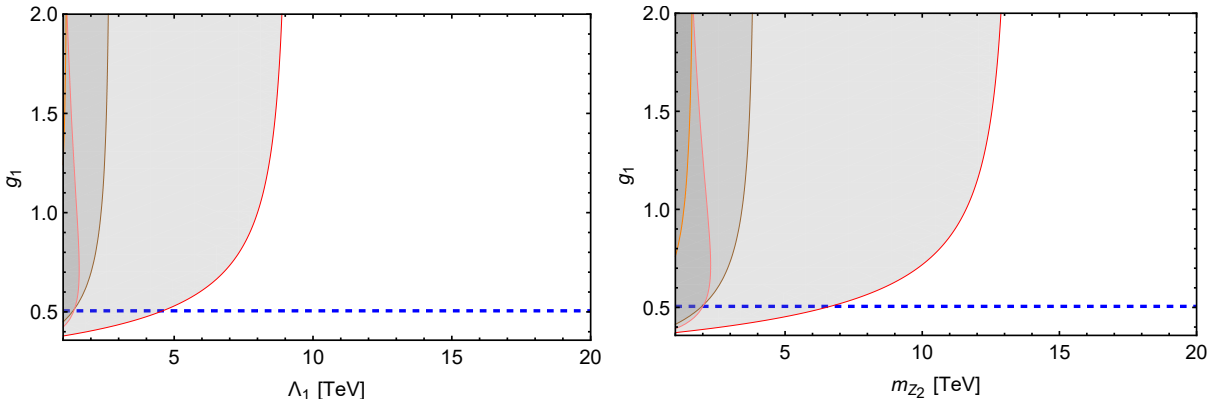


FIG. 2: The red, brown, pink, and orange curves represent the exclusion bounds derived from the Z -boson mass shift [1], the ρ parameter [1], the Z - Z' mixing parameter ε [36, 37], and the total decay width of Z_1 [1], respectively. The shaded regions are excluded by current experimental data. The dashed blue line indicates the gauge coupling unification condition $g_1 = g_2 = \sqrt{2}g_Y$.

B. FCNCs

Because the right-handed fermions carry non-universal charges under the $U(1)_Y \otimes U(1)_R$ gauge group, our model naturally generates tree-level Flavor-Changing Neutral Current (FCNC) processes, which serve as a key signature of new physics. These include $\Delta F = 2$ observables such as $\bar{B}_s - B_s$ and $\bar{B}_d - B_d$ mixing, as well as rare decays like $B_s \rightarrow \ell^+ \ell^-$, all mediated by the neutral gauge boson Z' . Furthermore, the Yukawa interactions in Eq. (39) induce flavor-changing scalar interactions via the neutral scalars H , \mathcal{H} , and \mathcal{A} , providing additional contributions to FCNC observables. In this section, we investigate a set of these observables arising from both the Z' boson and the neutral scalar fields.

For the FCNCs induced by the Z' gauge boson, the relevant interactions are given by

$$\mathcal{L} \supset \bar{q}_{\alpha R} i \gamma^\mu (i g_1 \mathcal{Y}_{q_{\alpha R}} B_{1\mu} + i g_2 \mathcal{R}_{q_{\alpha R}} B_{2\mu}) q_{\alpha R} + \bar{q}_{3R} i \gamma^\mu (i g_1 \mathcal{Y}_{q_{3R}} B_{1\mu} + i g_2 \mathcal{R}_{q_{3R}} B_{2\mu}) q_{3R}, \quad (60)$$

where $q = u, d$. The gauge fields $B_{1\mu}$ and $B_{2\mu}$ are related to the physical neutral gauge bosons Z_μ and Z'_μ through the relations $B_{1\mu} = -s_W s_\theta Z_\mu + c_\theta Z'_\mu$, $B_{2\mu} = -s_W c_\theta Z_\mu - s_\theta Z'_\mu$. Substituting these relations into Eq. (60) and transforming to the mass eigenbasis, where $q_{L,R} = V_{qL,R} q'_{L,R}$, we obtain the FCNC interactions,

$$\mathcal{L}_{\text{FCNC}}^{\text{gauge}} = \bar{q}'_{iR} [\Gamma_{qR}^{Z'}]_{ij} q_{jR} \gamma^\mu Z'_\mu, \quad (61)$$

where $[\Gamma_{qR}^{Z'}]_{ij}$ denote the flavor-violating couplings induced by the Z'_μ gauge boson,

$$[\Gamma_{qR}^{Z'}]_{ij} = \pm (g_1 c_\theta + g_2 s_\theta) z \sum_{\alpha=1,2} [V_{qR}^*]_{\alpha i} [V_{qR}]_{\alpha j}, \quad (62)$$

and the sign $+(-)$ corresponds to up-type (down-type) quarks. The quark mixing matrices $V_{qL,R}$ are numerically obtained from benchmark points given in Eqs. (53) and (54).

Besides, the model also includes FCNC sources arising from scalar exchanges. These contributions originate from the Yukawa interactions given in Eq. (39). For the scalar components $\Phi_1^0 \simeq \frac{1}{\sqrt{2}}[v_1 + H + i(c_\varphi G_Z + s_\varphi \mathcal{A})]$ and $\Phi_2^0 \simeq \frac{1}{\sqrt{2}}[v_2 + \mathcal{H} + i(s_\varphi G_Z - c_\varphi \mathcal{A})]$, the flavor-changing scalar interactions can be written as

$$\mathcal{L}_{\text{FCNC}}^{\text{scalar}} = -\bar{f}'_i [\Gamma_{fR}^H]_{ij} P_R f'_j H - \bar{f}'_i [\Gamma_{fR}^{\mathcal{H}}]_{ij} P_R f'_j \mathcal{H} - i \bar{f}'_i [\Gamma_{fR}^{\mathcal{A}}]_{ij} P_R f'_j \mathcal{A} + \text{H.c.}, \quad (63)$$

where $P_R = \frac{1}{2}(1 + \gamma_5)$, $f = u, d, e$, and the corresponding flavor-violating couplings are given by

$$[\Gamma_{fR}^H]_{ij} = \frac{1}{v_1} \sum_{k=1}^3 \sum_{a=1}^3 [V_{fL}^*]_{ai} [V_{fL}]_{ak} M_k^f [V_{fR}]_{3k} [V_{fR}]_{3j}, \quad (64)$$

$$[\Gamma_{fR}^{\mathcal{H}}]_{ij} = \frac{1}{v_2} \sum_{k=1}^3 \sum_{a=1}^3 \sum_{\alpha=1}^2 [V_{fL}^*]_{ai} [V_{fL}]_{\alpha k} M_k^f [V_{fR}]_{\alpha k} [V_{fR}]_{\alpha j}, \quad (65)$$

$$[\Gamma_{fR}^{\mathcal{A}}]_{ij} = \frac{\pm g}{2m_W} \sum_{k=1}^3 \sum_{a=1}^3 \sum_{\alpha=1}^2 \left\{ t_\varphi [V_{fL}^*]_{ai} [V_{fL}]_{ak} M_k^f [V_{fR}]_{3k} [V_{fR}]_{3j} \right. \\ \left. - \frac{1}{t_\varphi} [V_{fL}^*]_{ai} [V_{fL}]_{\alpha k} M_k^f [V_{fR}]_{\alpha k} [V_{fR}]_{\alpha j} \right\}, \quad (66)$$

with the positive (negative) sign corresponding to $f = e, d$ ($f = u$).

For the $\Delta F = 2$ flavor-changing processes, the effective Hamiltonian can be written as

$$\mathcal{H}_{\text{eff}}^{\Delta F=2} = \frac{G_F^2 m_W^2 (V_{tq}^* V_{tb})^2}{16\pi^2} [C_{\text{SM}}^q (\bar{b}_L \gamma_\mu q_L)^2 + C_{RR}^q (\bar{b}_R \gamma_\mu q_R)^2 + \tilde{C}_{LL}^q (\bar{b}_R q_L)^2 \\ + \tilde{C}_{RR}^q (\bar{b}_L q_R)^2 + \tilde{C}_{LR}^q (\bar{b}_R q_L)(\bar{b}_L q_R)], \quad (67)$$

where α and β denote color indices. The Wilson coefficients (WCs) C_{SM}^q represent the SM contribution to the $\bar{B}_q - B_q$ meson mixings and are given by [39]

$$C_{\text{SM}}^q = 4S_0(x_t) \eta_{2B}, \quad (68)$$

where $S_0(m_i^2/m_W^2)$ is the Inami-Lim function [40], and $\eta_{2B} \simeq 0.84$ accounts for the next-to-leading order (NLO) QCD corrections [41].² It is worth emphasizing that only the right-handed fermions carry non-universal charges under the gauge group $U(1)_Y \otimes U(1)_R$. As a result, the NP contributions from the additional gauge boson Z' affect solely the WC C_{RR}^q . The NP WCs C_{RR}^q and $\tilde{C}_{LL,RR,LR}^q$ are defined at the matching scale $\mu = m_{Z'}$:

$$C_{RR}^q = \frac{16\pi^2}{G_F^2 m_W^2 (V_{tq}^* V_{tb})^2} \frac{([\Gamma_{dR}^{Z'}]_{3q})^2}{m_{Z'}^2}, \quad (69)$$

$$\tilde{C}_{LL}^q = \frac{-16\pi^2}{G_F^2 m_W^2 (V_{tq}^* V_{tb})^2} \left[\frac{([\Gamma_{dR}^H]_{q3})^2}{m_H^2} + \frac{([\Gamma_{dR}^{\mathcal{H}}]_{q3})^2}{m_{\mathcal{H}}^2} - \frac{([\Gamma_{dR}^{\mathcal{A}}]_{q3})^2}{m_{\mathcal{A}}^2} \right], \quad (70)$$

$$\tilde{C}_{RR}^q = \frac{-16\pi^2}{G_F^2 m_W^2 (V_{tq}^* V_{tb})^2} \left[\frac{([\Gamma_{dR}^H]_{3q})^2}{m_H^2} + \frac{([\Gamma_{dR}^{\mathcal{H}}]_{3q})^2}{m_{\mathcal{H}}^2} - \frac{([\Gamma_{dR}^{\mathcal{A}}]_{3q})^2}{m_{\mathcal{A}}^2} \right], \quad (71)$$

$$\tilde{C}_{LR}^q = \frac{-32\pi^2}{G_F^2 m_W^2 (V_{tq}^* V_{tb})^2} \left[\frac{[\Gamma_{dR}^H]_{3q} [\Gamma_{dR}^H]_{q3}^*}{m_H^2} + \frac{[\Gamma_{dR}^{\mathcal{H}}]_{3q} [\Gamma_{dR}^{\mathcal{H}}]_{q3}^*}{m_{\mathcal{H}}^2} + \frac{[\Gamma_{dR}^{\mathcal{A}}]_{3q} [\Gamma_{dR}^{\mathcal{A}}]_{q3}^*}{m_{\mathcal{A}}^2} \right], \quad (72)$$

where the flavor-violating couplings $[\Gamma_{dL,R}^{Z'}]_{ij}$ and $[\Gamma_{dL,R}^{H,\mathcal{H},\mathcal{A}}]_{ij}$ are defined in Eq. (62) and Eqs. (64)–(66), respectively. With the effective Hamiltonian for $\Delta F = 2$ processes given in Eq. (67), the ratio between the SM+NP and SM contributions to the meson mass differences can be expressed as

$$\begin{aligned} \epsilon_{B_q} &= \frac{\Delta m_{B_q}^{\text{SM+NP}}}{\Delta m_{B_q}^{\text{SM}}} = \left| 1 + \frac{M_{12}^{q,\text{NP}}}{M_{12}^{q,\text{SM}}} \right| \\ &= \left| 1 + \frac{C_{RR}^q \eta_{B_q}^{6/23}}{C_{\text{SM}}^q} + \frac{(\tilde{C}_{RR}^q + \tilde{C}_{LL}^q)}{C_{\text{SM}}^q} \left(\frac{m_{B_q}}{m_b + m_q} \right)^2 \left(\frac{-5B_{B_q}^{(2)} \eta_{22} + B_{B_q}^{(3)} \eta_{32}}{12B_{B_q}^{(1)}} \right) \right. \\ &\quad \left. + \frac{\tilde{C}_{LR}^q}{C_{\text{SM}}^q} \left[\frac{1}{6} + \left(\frac{m_{B_q}}{m_b + m_q} \right)^2 \right] \eta_4 \frac{B_{B_q}^{(4)}}{B_{B_q}^{(1)}} \right|. \end{aligned} \quad (73)$$

Here, $\eta_{22} = 0.983 \eta_{B_q}^{-0.63} + 0.017 \eta_{B_q}^{0.717}$, $\eta_{32} = -0.064 \eta_{B_q}^{-0.63} + 0.064 \eta_{B_q}^{0.717}$, and $\eta_4 = \eta_{B_q}^{-24/23}$, where the coefficient $\eta_{B_q} = \alpha_s(\mu_{\text{NP}})/\alpha_s(\mu_{B_q})$ represents the leading-order (LO) QCD correction obtained via renormalization group evolution (RGE) from the new-physics scale $\mu_{\text{NP}} = m_{\text{NP}}$ down to the hadronic scale $\mu_{B_q} = 4.16$ GeV [42]. The impact of NP on the mass difference Δm_{B_q} can then be constrained by the 2σ experimental ranges given in Ref. [33]:

$$\frac{\Delta m_{B_s}^{\text{SM+NP}}}{\Delta m_{B_s}^{\text{SM}}} = \frac{\Delta m_{B_s}^{\text{exp}}}{\Delta m_{B_s}^{\text{SM}}} \in [0.9072, 1.0419], \quad (74)$$

$$\frac{\Delta m_{B_d}^{\text{SM+NP}}}{\Delta m_{B_d}^{\text{SM}}} = \frac{\Delta m_{B_d}^{\text{exp}}}{\Delta m_{B_d}^{\text{SM}}} \in [0.8728, 1.0222]. \quad (75)$$

We also emphasize that our model predicts NP contributions to the $\Delta S = 1$ rare decay $B_s \rightarrow \mu^+ \mu^-$ at tree-level. This decay can be described by the effective Hamiltonian

$$\mathcal{H}_{\text{eff}}^{\Delta S=1} = -\frac{4G_F V_{ts}^* V_{tb}}{\sqrt{2}} [C_{10}^{\text{SM}} (\bar{s}_L \gamma_\mu b_L) (\bar{\mu} \gamma^\mu \gamma_5 \mu) + C_{10}' (\bar{s}_R \gamma_\mu b_R) (\bar{\mu} \gamma^\mu \gamma_5 \mu) \sum_{i=S,P} (C_i \mathcal{O}_i + C'_i \mathcal{O}'_i)], \quad (76)$$

where the scalar and pseudoscalar operators induced by the neutral scalars H, \mathcal{H} and \mathcal{A} are defined as

$$\mathcal{O}_S = \frac{e^2}{16\pi^2} (\bar{s} P_R b) (\bar{\mu} \mu), \quad \mathcal{O}'_S = \frac{e^2}{16\pi^2} (\bar{s} P_L b) (\bar{\mu} \mu), \quad (77)$$

$$\mathcal{O}_P = \frac{e^2}{16\pi^2} (\bar{s} P_R b) (\bar{\mu} \gamma_5 \mu), \quad \mathcal{O}'_P = \frac{e^2}{16\pi^2} (\bar{s} P_L b) (\bar{\mu} \gamma_5 \mu). \quad (78)$$

² For the K meson, the SM prediction Δm_K^{SM} suffers from large and poorly controlled theoretical uncertainties due to long-distance effects. Consequently, the constraint from Δm_K is weaker than those from $\Delta m_{B_{s,d}}$, and it is therefore omitted in the present analysis.

Since the FCNCs associated with the new gauge boson Z' only arise from the right-handed sector, there is no NP contribution to the left-handed operator $(\bar{s}_L \gamma_\mu b_L)(\bar{\mu} \gamma^\mu \gamma_5 \mu)$, similar to the case of the $\Delta S = 2$ observables. In the SM, the WC C_{10}^{SM} has been computed up to next-to-next-to-leading order (NNLO) in QCD, with a numerical value of $C_{10}^{\text{SM}} = -4.194$. The non-SM WCs are given by

$$C'_{10} = -\frac{16\pi^2}{e^2} \frac{g\sqrt{2}}{8c_W G_F V_{ts}^* V_{tb}} \frac{[\Gamma_{dR}^{Z'}]_{23} [\tilde{g}_A^{Z'}]_{22}}{m_{Z'}^2}, \quad (79)$$

$$C_S = \frac{16\pi^2}{e^2} \frac{\sqrt{2}}{4G_F V_{ts}^* V_{tb}} \left[\frac{[\Gamma_{dR}^H]_{23} \text{Re}([\Gamma_{eR}^H]_{22})}{m_H^2} + \frac{[\Gamma_{dR}^H]_{23} \text{Re}([\Gamma_{eR}^H]_{22})}{m_H^2} - i \frac{[\Gamma_{dR}^A]_{23} \text{Im}([\Gamma_{eR}^A]_{22})}{m_A^2} \right], \quad (80)$$

$$C'_S = \frac{16\pi^2}{e^2} \frac{\sqrt{2}}{4G_F V_{ts}^* V_{tb}} \left[\frac{[\Gamma_{dR}^H]_{32}^* \text{Re}([\Gamma_{eR}^H]_{22})}{m_H^2} + \frac{[\Gamma_{dR}^H]_{32}^* \text{Re}([\Gamma_{eR}^H]_{22})}{m_H^2} + i \frac{[\Gamma_{dR}^A]_{32}^* \text{Im}([\Gamma_{eR}^A]_{22})}{m_A^2} \right], \quad (81)$$

$$C_P = -\frac{16\pi^2}{e^2} \frac{\sqrt{2}}{4G_F V_{ts}^* V_{tb}} \left[\frac{[\Gamma_{dR}^A]_{23} \text{Re}([\Gamma_{eR}^A]_{22})}{m_A^2} - i \frac{[\Gamma_{dR}^H]_{23} \text{Im}([\Gamma_{eR}^H]_{22})}{m_H^2} - i \frac{[\Gamma_{dR}^H]_{23} \text{Im}([\Gamma_{eR}^H]_{22})}{m_H^2} \right], \quad (82)$$

$$C'_P = \frac{16\pi^2}{e^2} \frac{\sqrt{2}}{4G_F V_{ts}^* V_{tb}} \left[\frac{[\Gamma_{dR}^A]_{32}^* \text{Re}([\Gamma_{eR}^A]_{22})}{m_A^2} + i \frac{[\Gamma_{dR}^H]_{32}^* \text{Im}([\Gamma_{eR}^H]_{22})}{m_H^2} + i \frac{[\Gamma_{dR}^H]_{32}^* \text{Im}([\Gamma_{eR}^H]_{22})}{m_H^2} \right]. \quad (83)$$

The branching ratio for the rare decay $B_s \rightarrow \mu^+ \mu^-$ is given by

$$\begin{aligned} \epsilon_{B_s \rightarrow \mu^+ \mu^-} &= \frac{\text{BR}(B_s \rightarrow \mu^+ \mu^-)_{\text{SM+NP}}}{\text{BR}(B_s \rightarrow \mu^+ \mu^-)_{\text{SM}}} = \frac{\text{BR}(B_s \rightarrow \mu^+ \mu^-)_{\text{exp}}}{\text{BR}(B_s \rightarrow \mu^+ \mu^-)_{\text{SM}}} \\ &= \frac{1 + \mathcal{A}_{\Delta\Gamma} y_s}{1 - y_s^2} \frac{|P|^2 + |S|^2}{|C_{10}^{\text{SM}}|^2}, \end{aligned} \quad (84)$$

where the parameters P and S are defined as

$$P = C_{10}^{\text{SM}} - C'_{10} + \frac{m_{B_s}^2}{2m_\mu(m_b + m_s)} (C_P - C'_P), \quad (85)$$

$$S = \sqrt{1 - \frac{4m_\mu^2}{m_{B_s}^2} \frac{m_{B_s}^2}{2m_\mu(m_b + m_s)} (C_S - C'_S)}. \quad (86)$$

Here, the observable $\mathcal{A}_{\Delta\Gamma}$ takes the value 1 in the SM. In the presence of NP contributions, it is modified as follows [43]

$$\mathcal{A}_{\Delta\Gamma} = \frac{|P|^2 \cos(2\phi_P - \phi_s^{\text{NP}}) - |S|^2 \cos(2\phi_S - \phi_s^{\text{NP}})}{|P|^2 + |S|^2}. \quad (87)$$

To estimate the impact of NP, we consider the predicted ratio $\epsilon_{B_s \rightarrow \mu^+ \mu^-}$ constrained by the experimental measurement within the corresponding 2σ range,

$$\frac{\text{BR}(B_s \rightarrow \mu^+ \mu^-)_{\text{exp}}}{\text{BR}(B_s \rightarrow \mu^+ \mu^-)_{\text{SM}}} \in [0.7574, 1.0778], \quad (88)$$

where the experimental branching ratio is $\text{BR}(B_s \rightarrow \mu^+ \mu^-)_{\text{exp}} = 3.34(27) \times 10^{-9}$ [44], and the SM prediction, including power-enhanced QED corrections, is $\text{BR}(B_s \rightarrow \mu^+ \mu^-)_{\text{SM}} = 3.64(12) \times 10^{-9}$ [1].

For the numerical analysis, we fix $z = 1$, $\Lambda_1 = \Lambda_2$, and $v_2 = 0.52$ GeV, consistent with the fit to the SM fermion mass spectrum and mixing parameters. Fig. 3 illustrates the dependence of the lower bound of the Higgs coupling $-\mu_0^2$ on the new-physics scale Λ_1 for several values of the $U(1)_Y$ gauge coupling g_1 .³ Here, the gray-shaded region is excluded by the 2σ experimental constraints from Δm_{B_q} and $\text{BR}(B_s \rightarrow \mu^+ \mu^-)$, given in Eqs. (74), (75), and (88), while the white region remains allowed. For Λ_1 in the few-TeV range, the lower bound $-\mu_0^2 \gtrsim 1.84 \times 10^4$ GeV 2 is controlled by the constraint from $\epsilon_{B_s \rightarrow \mu^+ \mu^-}$, which depends only mildly on Λ_1 and g_1 . This value is consistent with the theoretical expectation $-\mu_0^2 \sim \mathcal{O}(10^4)$ GeV 2 , estimated from the loop correction to the $\mu_0^2 \Phi_1^\dagger \Phi_2$ term in the scalar

³ The gauge couplings g_1 and g_2 are related by $g_2 = g_1 g_Y / \sqrt{g_1^2 - g_Y^2}$, requiring $g_1 \geq g_Y$ to ensure a real and positive value of g_2 .

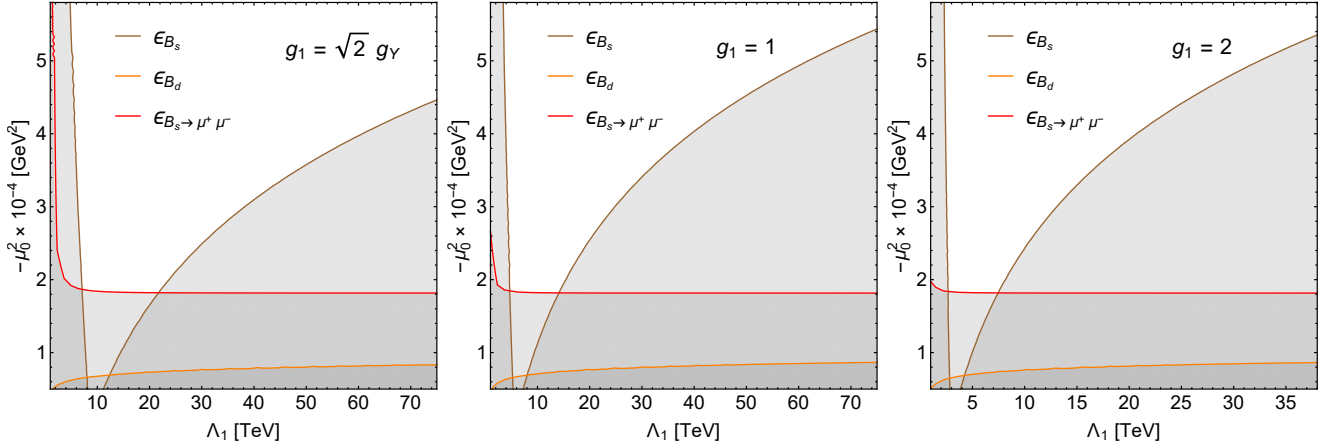


FIG. 3: Lower bounds of $-\mu_0^2$ as a function of the new-physics scale Λ_1 for several values of g_1 . The gray-shaded region is excluded by the 2σ flavor constraints, while the white region is allowed.

potential (see Appendix A). At larger Λ_1 , however, the lower bound on $-\mu_0^2$ is instead governed by the ϵ_{B_s} constraint, which exhibits a stronger dependence on both Λ_1 and g_1 . Although the direct Z' -mediated contributions—through the Wilson coefficients C_{RR}^q and C_{10}' —are numerically much smaller than the scalar-mediated ones ($H, \mathcal{H}, \mathcal{A}$), the overall B_q – \bar{B}_q mixing amplitude still retains a nontrivial dependence on Λ_1 through the factor η_{B_q} . As Λ_1 increases, this dependence requires a larger magnitude of $-\mu_0^2$ to compensate and keep the total mixing amplitude within the experimentally allowed range. Finally, Fig. 3 also implies a conservative lower bound on the new-physics scale, $\Lambda_1 \gtrsim \mathcal{O}(1)$ TeV.

C. Collider signatures

1. Z' Production at Proton–Proton Colliders

We analyze the Drell–Yan production of the heavy Z' gauge boson at the LHC. The Z' gauge boson is primarily produced at the LHC through the Drell–Yan process, with the light quarks u, d, s providing the dominant parton distribution functions (PDF) contributions. The total $pp \rightarrow Z'$ cross section at \sqrt{S} energy, mediated by $q\bar{q}$ annihilation can be expressed as:

$$\begin{aligned} \sigma_{pp \rightarrow Z'}^{(\text{DrellYan})}(S) = & \frac{g^2 \pi}{12 c_W^2 S} \left\{ \left[\left(g_V^{Z_2}(u_\alpha) \right)^2 + \left(g_A^{Z_2}(u_\alpha) \right)^2 \right] \int_{\ln \sqrt{\frac{m_{Z'}^2}{S}}}^{-\ln \sqrt{\frac{m_{Z'}^2}{S}}} f_{p/u} \left(\sqrt{\frac{m_{Z'}^2}{S}} e^y, \mu^2 \right) f_{p/\bar{u}} \left(\sqrt{\frac{m_{Z'}^2}{S}} e^{-y}, \mu^2 \right) dy \right. \\ & + \left[\left(g_V^{Z_2}(d_\alpha) \right)^2 + \left(g_A^{Z_2}(d_\alpha) \right)^2 \right] \int_{\ln \sqrt{\frac{m_{Z'}^2}{S}}}^{-\ln \sqrt{\frac{m_{Z'}^2}{S}}} f_{p/d} \left(\sqrt{\frac{m_{Z'}^2}{S}} e^y, \mu^2 \right) f_{p/\bar{d}} \left(\sqrt{\frac{m_{Z'}^2}{S}} e^{-y}, \mu^2 \right) dy \\ & \left. + \left[\left(g_V^{Z_2}(s_\alpha) \right)^2 + \left(g_A^{Z_2}(s_\alpha) \right)^2 \right] \int_{\ln \sqrt{\frac{m_{Z'}^2}{S}}}^{-\ln \sqrt{\frac{m_{Z'}^2}{S}}} f_{p/s} \left(\sqrt{\frac{m_{Z'}^2}{S}} e^y, \mu^2 \right) f_{p/\bar{s}} \left(\sqrt{\frac{m_{Z'}^2}{S}} e^{-y}, \mu^2 \right) dy \right\}, \quad (89) \end{aligned}$$

where the functions $f_{p/u}(x_1, \mu^2)$ ($f_{p/\bar{u}}(x_2, \mu^2)$), $f_{p/d}(x_1, \mu^2)$ ($f_{p/\bar{d}}(x_2, \mu^2)$) and $f_{p/s}(x_1, \mu^2)$ ($f_{p/\bar{s}}(x_2, \mu^2)$) correspond to the parton distribution functions of the light up, down and strange quarks (antiquarks), respectively, in the proton which carry momentum fractions x_1 (x_2) of the proton. The factorization scale is taken to be $\mu = m_{Z'}$.

Fig. 4 displays the total cross section at the LHC for the Z' production via the Drell–Yan mechanism for $\sqrt{S} = 14$ TeV (left plot) and $\sqrt{S} = 28$ TeV (right plot) as a function of the Z' mass $m_{Z'}$, which is taken to range from 5 TeV up to 7 TeV. Here we have set $z = 1$, $\theta = 0.45\pi$ and $\Lambda_1 = \Lambda_2 = 10$ TeV. We focus on values of Z' gauge boson mass

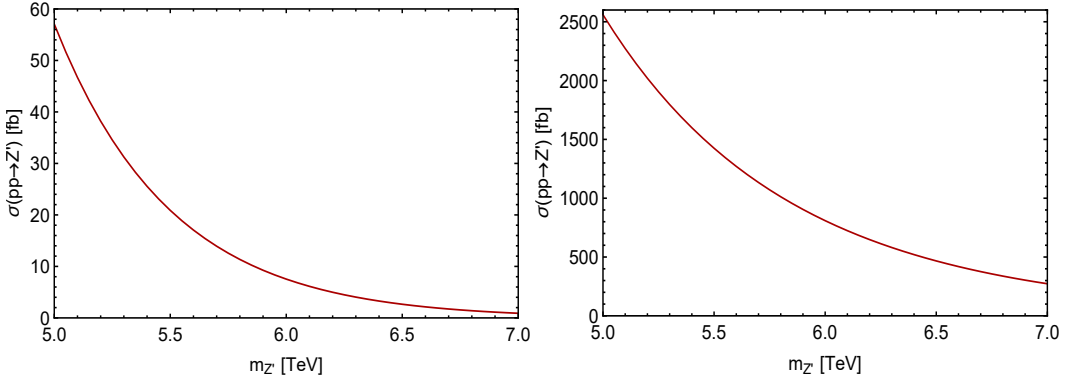


FIG. 4: Total cross section for Z' production via Drell–Yan mechanism at the LHC as a function of the Z' mass, for $\sqrt{S} = 14$ TeV (left) and $\sqrt{S} = 28$ TeV (right).

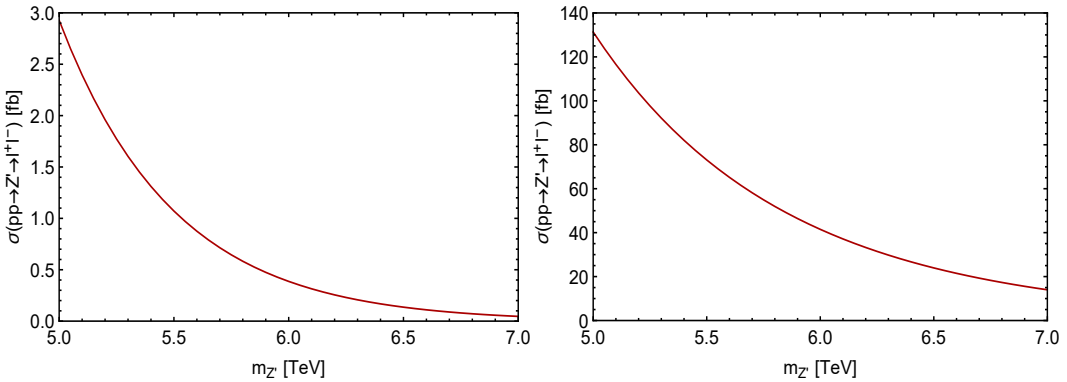


FIG. 5: Total cross section for resonant $pp \rightarrow Z' \rightarrow l^+l^-$ production via Drell–Yan mechanism at the LHC as a function of the Z' mass, for $\sqrt{S} = 14$ TeV (left) and $\sqrt{S} = 28$ TeV (right).

above 5 TeV, choice compatible with the constraint $\frac{M_{Z'}}{g} > 7$ TeV ($g \approx 0.65$), derived from LEP I/II measurements of $e^+e^- \rightarrow l^+l^-$ [45–47] and supported by LHC searches [48, 49]. Further bounds on $\frac{M_{Z'}}{g}$ for LEP II and projected scenarios at future e^+e^- colliders (e.g., ILC) are analyzed in Ref. [47]. For our analysis, we apply the conservative LEP II limit, as other bounds depend on unrealized future experiments. Within the above mentioned Z' mass range, the total production cross section spans 57 fb to 0.9 fb at $\sqrt{S} = 14$ TeV. For the 28 TeV LHC upgrade, the cross section rises from 2560 fb down to 273 fb as seen in the right panel of Fig. 4. The Z' predominantly decays into SM fermion pairs, making dilepton or dijet excesses a potential discovery channel at the LHC. The total cross sections for the $pp \rightarrow Z' \rightarrow l^+l^-$ resonance production via Drell–Yan mechanism at a proton–proton collider for $\sqrt{S} = 14$ TeV and $\sqrt{S} = 28$ TeV are shown in the left and right panels of Fig. 5, respectively. The corresponding cross sections vary from 2.9 fb to 0.05 fb at $\sqrt{S} = 14$ TeV, and from 131 fb to 14 fb at $\sqrt{S} = 28$ TeV.

2. \mathcal{H} Scalar Production at Proton–Proton Colliders

We now examine the production mechanisms for the heavy neutral scalar, denoted \mathcal{H} , in proton–proton (pp) collisions. The gluon fusion process represents the most significant production channel at the LHC, proceeding through a top and charm quark loops. The corresponding cross section for $pp \rightarrow \mathcal{H}$ at a center-of-mass energy \sqrt{S} is

expressed as:

$$\begin{aligned} \sigma_{pp \rightarrow gg \rightarrow \mathcal{H}}(S) = & \frac{\alpha_S^2 m_{\mathcal{H}}^2}{64\pi S} \left[\frac{a_{\mathcal{H}t\bar{t}}}{v_1} I\left(\frac{m_{\mathcal{H}}^2}{m_t^2}\right) + \frac{a_{\mathcal{H}c\bar{c}}}{v_2} I\left(\frac{m_{\mathcal{H}}^2}{m_c^2}\right) \right]^2 \\ & \times \int_{\ln \sqrt{\frac{m_{\mathcal{H}}^2}{S}}}^{-\ln \sqrt{\frac{m_{\mathcal{H}}^2}{S}}} f_{p/g} \left(\sqrt{\frac{m_{\mathcal{H}}^2}{S}} e^y, \mu^2 \right) f_{p/g} \left(\sqrt{\frac{m_{\mathcal{H}}^2}{S}} e^{-y}, \mu^2 \right) dy, \end{aligned} \quad (90)$$

where the functions $f_{p/g}(x_1, \mu^2)$ and $f_{p/g}(x_2, \mu^2)$ describe the gluon density within the proton, carrying momentum fractions x_1 and x_2 , respectively. The factorization scale is chosen as $\mu = m_{\mathcal{H}}$. The loop function $I(z)$, which arises from the top-quark loop, is given by the integral:

$$I(z) = \int_0^1 dx \int_0^{1-x} dy \frac{1-4xy}{1-zxy}. \quad (91)$$

The resulting production cross sections are displayed in the subsequent figures. The dependence of the \mathcal{H} production cross section on its mass is plotted in the left panel of Fig. 6 for the LHC operating at $\sqrt{S} = 14$ TeV, considering a mass range from 0.4 TeV to 1 TeV. For this calculation, the Yukawa couplings $a_{\mathcal{H}t\bar{t}}$ and $a_{\mathcal{H}c\bar{c}}$ are fixed to 0.1 and 1, respectively. Besides that we have set $v_2 = 0.5$ GeV and $v_1 = \sqrt{v^2 - v_2^2} \approx 246$ GeV. Within this mass window, the cross section falls from about 417 fb to 3.2 fb.

Significant enhancements in the production rate are anticipated at higher collision energies. The right panel of Fig. 6 illustrates the cross section for a potential future LHC run at $\sqrt{S} = 28$ TeV, where it spans from 1730 fb down to 22 fb across the same \mathcal{H} mass range. From a phenomenological perspective, if \mathcal{H} is the lightest beyond-the-Standard-Model scalar, it decays predominantly to pairs of first- and second-generation quarks or charged leptons. These decay channels would yield final states rich in jets and/or leptons. It is crucial to note, however, that our analysis is conducted near the alignment limit, where the coupling of the SM light Higgs boson H are very close to the SM expectation. Consequently, the contribution from \mathcal{H} pair production to multilepton and multijet signals is predicted to be minor compared to the dominant SM processes.

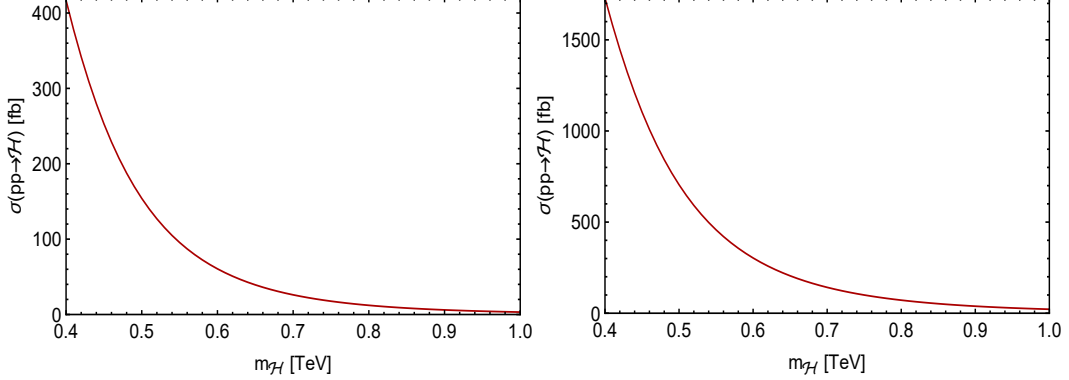


FIG. 6: Total cross section for \mathcal{H} production via gluon fusion at a proposed pp collider as a function of $m_{\mathcal{H}}$, for $\sqrt{S} = 14$ TeV (left) and $\sqrt{S} = 28$ TeV (right).

V. COMPLEX SCALAR SINGLET DARK MATTER

This model features a residual parity P_D under which the scalars ϕ^0 , η_1 , and η_2 are odd. The conserved residual parity P_D stabilizes the lightest such state, identifying it as a DM candidate. The mass of this candidate is naturally heavy (typically TeV-scale), being determined by the breaking scales $\Lambda_{1,2}$. The DM interacts with SM particles through contact terms in the scalar potential, as well as via scalar and gauge portals. Consequently, its relic abundance is governed by the thermal freeze-out mechanism, implying WIMP-like behavior. For simplicity, we assume the DM candidate to be the lightest state in the spectrum beyond the SM, with the possible exception of the physical Goldstone boson \mathcal{G} .

A. Dark matter as a complex scalar singlet η_2

We first consider the scenario in which the complex scalar singlet η_2 acts as the DM candidate. Since η_2 is an $SU(2)_L$ singlet with both $\mathcal{Y} = 0$ and $\mathcal{R} = 0$, the Z_1 and Z_2 annihilation portals are absent. The Z_R portal is also negligible due to the mass hierarchy, namely $m_{\eta_2} \ll m_{Z_R}$. Furthermore, the $\mathcal{H}_{1,2}$ portals can be ignored under the assumption $|\lambda_{30,31}| \ll 1$ as they do not contribute to direct DM detection. Consequently, η_2 predominantly annihilates into SM particles through the contact interaction $\frac{1}{2}\lambda_{28}\eta_2^*\eta_2 H^2$, as well as via the scalar portals mediated by H and \mathcal{H} . The corresponding thermally averaged annihilation cross section is then given by:

$$\begin{aligned} \langle\sigma v_{\text{rel}}\rangle_{\eta_2^*\eta_2} &= \langle\sigma v_{\text{rel}}\rangle_{\eta_2^*\eta_2 \rightarrow HH} + \langle\sigma v_{\text{rel}}\rangle_{\eta_2^*\eta_2 \rightarrow ff^c} + \langle\sigma v_{\text{rel}}\rangle_{\eta_2^*\eta_2 \rightarrow W^+W^-, Z_1Z_1} \\ &\simeq \frac{1}{32\pi m_{\eta_2}^2} \left[\lambda_{28} + \frac{\lambda^2 \Lambda_2^2}{4(m_{\eta_2}^2 + m_{\phi^0}^2)} + \frac{3\lambda_{28}\lambda_1 v_1^2}{4m_{\eta_2}^2} + \frac{\lambda_{29}(\lambda_3 + \lambda_4)v_2^2}{4m_{\eta_2}^2 - m_{\mathcal{H}}^2} \right]^2 \\ &\quad + \frac{3m_t^2}{\pi} \left[\frac{\lambda_{28}}{4m_{\eta_2}^2} + \frac{\lambda_{29}\epsilon_1 v_2}{(4m_{\eta_2}^2 - m_{\mathcal{H}}^2)v_1} \right]^2 + \frac{3}{16\pi m_{\eta_2}^2 v^4} \left(\lambda_{28}v_1^2 + \frac{4\lambda_{29}v_2^2 m_{\eta_2}^2}{4m_{\eta_2}^2 - m_{\mathcal{H}}^2} \right)^2. \end{aligned} \quad (92)$$

The scattering of η_2 off a nuclear target is primarily mediated by the t -channel exchange of the scalar bosons H and \mathcal{H} . The effective Lagrangian describing this interaction at the quark level is given by

$$\mathcal{L}_{\eta_2\text{-quark}}^{\text{eff,scalar}} = C_{\eta_2 q}^S \eta_2^* \eta_2 \bar{q} q = m_q \left(\frac{C_q^H}{m_H^2} + \frac{C_q^{\mathcal{H}}}{m_{\mathcal{H}}^2} \right) \eta_2^* \eta_2 \bar{q} q, \quad (93)$$

where m_q is the mass of the quark q , and

$$C_u^H = C_c^H = C_d^H = C_s^H \simeq \frac{\lambda_{28}\epsilon_1 v_1}{v_2}, \quad C_t^H = C_b^H \simeq -\lambda_{28}, \quad (94)$$

$$C_u^{\mathcal{H}} = C_c^{\mathcal{H}} = C_d^{\mathcal{H}} = C_s^{\mathcal{H}} = -\frac{\lambda_{28}\epsilon_1 v_1 + \lambda_{29}v_2}{v_2}, \quad C_t^{\mathcal{H}} = C_b^{\mathcal{H}} = -\frac{\epsilon_1(\lambda_{28}\epsilon_1 v_1 + \lambda_{29}v_2)}{v_1}. \quad (95)$$

Then, at the nucleon level, the effective Lagrangian takes the form

$$\mathcal{L}_{\eta_2\text{-nucleon}}^{\text{eff,scalar}} = C_{\eta_2 N} \eta_2^* \eta_2 \bar{N} N, \quad (96)$$

in which $C_{\eta_2 N}$ ($N = p, n$) denotes the effective coupling of DM to nucleons (protons, neutrons). These effective couplings are given by

$$C_{\eta_2 N} = \frac{m_N}{2m_{\eta_2}} \left[\sum_{q=u,d,s} f_{Tq}^N \frac{C_{\eta_2 q}^S}{m_q} + \frac{2}{27} \left(1 - \sum_{q=u,d,s} f_{Tq}^N \right) \sum_{q=c,b,t} \frac{C_{\eta_2 q}^S}{m_q} \right], \quad (97)$$

where f_{Tq}^N are the scalar form factors of the nucleon for the quark q . The number values used in our analysis are $f_{Tu}^{p(n)} \simeq 0.0208(0.0189)$, $f_{Td}^{p(n)} \simeq 0.0411(0.0451)$, and $f_{Ts}^{p(n)} \simeq 0.043(0.043)$ [50, 51]. From this effective interaction, the spin-independent (SI) scattering cross-section of η_2 off a nuclear target \mathbb{A} is given by [52]

$$\sigma_{\eta_2\text{-}\mathbb{A}}^{\text{SI}} = \frac{\mu_{\mathbb{A}}^2}{\pi} [ZC_{\eta_2 p} + (A - Z)C_{\eta_2 n}]^2, \quad (98)$$

where $\mu_{\mathbb{A}} = \frac{m_{\mathbb{A}} m_{\eta_2}}{m_{\mathbb{A}} + m_{\eta_2}}$ is the reduced mass of the DM–nucleus system. Here, $m_{\mathbb{A}}$ denotes the mass of the target nucleus, Z is the atomic number, and A is the mass number.

We find that the ratio $C_{\eta_2 n}/C_{\eta_2 p}$ lies within the range of approximately 0.966–1.018 for representative parameter values: $\lambda_{29} = 0.1$, $v_2 = 0.52$ GeV, $m_{\eta_2} \sim \mathcal{O}(1)$ TeV, $\lambda_{28} = 0.001\text{--}1$, and $-\mu_0^2 = (0.4\text{--}10) \times 10^4$ GeV 2 . Accordingly, the SI DM–nucleon cross section, $\sigma_{\eta_2}^{\text{SI}}$, is related to the DM–nucleus cross section, $\sigma_{\eta_2\text{-}\mathbb{A}}^{\text{SI}}$, by $\sigma_{\eta_2}^{\text{SI}} = (\sigma_{\eta_2\text{-}\mathbb{A}}^{\text{SI}}/A^2)(\mu_p/\mu_{\mathbb{A}})^2$, where μ_p is the reduced mass of the DM–proton system [53].

Fig. 7 shows the correlation between the SI cross section $\sigma_{\eta_2}^{\text{SI}}$ and the DM mass m_{η_2} , yielding the correct DM relic abundance, $\Omega_{\eta_2} h^2 \simeq 0.1 \text{ pb}/\langle\sigma v_{\text{rel}}\rangle_{\eta_2^*\eta_2} \simeq 0.12$, as measured by the Planck experiment [4]. The numerical

results are obtained by setting $\lambda_{28} = \lambda_{29} = \lambda_3 = \lambda_4 = \lambda = 0.1$, $v_2 = 0.52$ GeV, $\Lambda_2 = 10$ TeV, $m_{\phi^0} = 2.5$ TeV, $Z = 54$, and $A = 131$, with $-\mu_0^2$ varying in the range $(0.4\text{--}10) \times 10^4$ GeV 2 . In the left panel, the mass region consistent with the relic density corresponds to the H -portal, which is nearly independent of μ_0^2 , leading to a relatively narrow allowed region. By contrast, the right panel shows the mass region associated with the \mathcal{H} -portal, which is strongly sensitive to μ_0^2 and results in a much broader allowed parameter space. For comparison, the most stringent experimental bounds from XENONnT [54], PandaX-4T [55], and LZ [56] are also displayed. The shaded black regions are excluded by these experiments, while the red-shaded region is excluded due to DM instability. Two viable mass regions for η_2 are identified: $m_{\eta_2} \simeq 624.7$ GeV for $-\mu_0^2 \simeq (1.23\text{--}5.86) \times 10^4$ GeV 2 (left panel), and $m_{\eta_2} \simeq (1.01\text{--}2.50)$ TeV for $-\mu_0^2 \simeq (0.87\text{--}5.28) \times 10^4$ GeV 2 (right panel). Furthermore, the projected sensitivities of upcoming direct-detection experiments imply even tighter constraints: $-\mu_0^2 \simeq (1.72\text{--}2.46) \times 10^4$ GeV 2 (left panel), and $m_{\eta_2} \simeq (1.26\text{--}2.50)$ TeV for $-\mu_0^2 \simeq (1.35\text{--}5.28) \times 10^4$ GeV 2 (right panel) [57–60]. Finally, the smallest value of $\sigma_{\eta_2}^{\text{SI}}$ is found at $-\mu_0^2 \simeq 2.02 \times 10^4$ GeV 2 (both panels), and $m_{\eta_2} \simeq 1.55$ TeV (right panel).

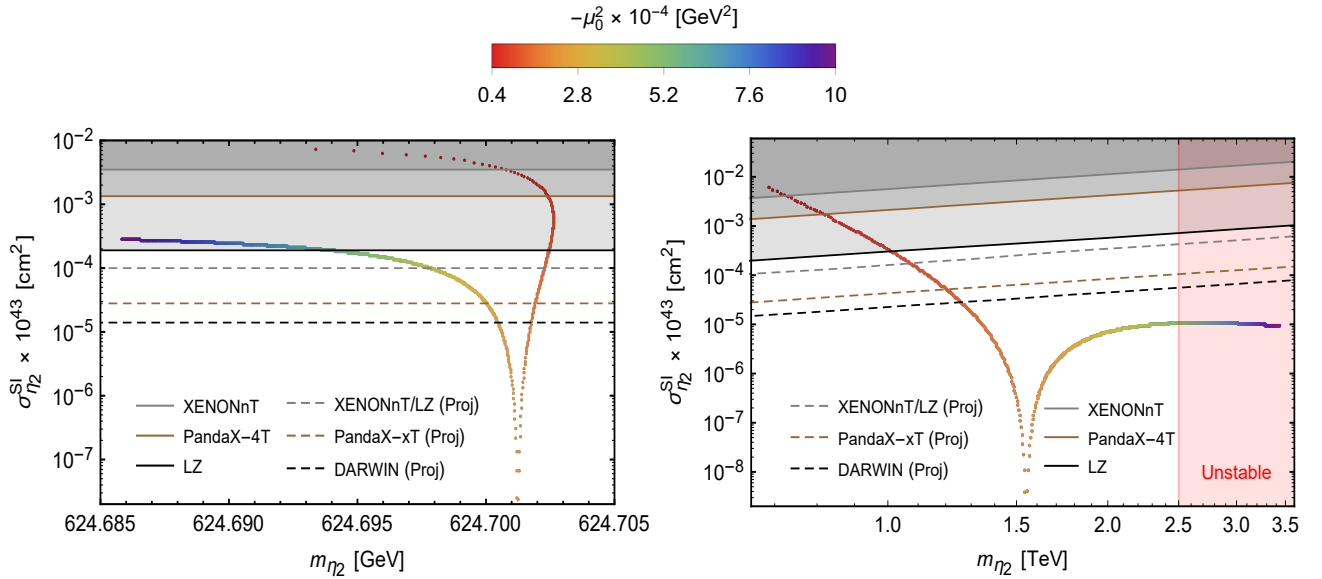


FIG. 7: The SI cross section of the DM candidate η_2 with nucleons as a function of its mass m_{η_2} , shown for various values of μ_0^2 . The shaded black regions are excluded by the XENONnT [54], PandaX-4T [55], and LZ [56] experiments, while the shaded red region is excluded due to the instability of η_2 . Projected sensitivities from future direct-detection experiments—XENONnT/LZ [57, 58], PandaX-xT [59], and DARWIN [60]—are indicated by the green, brown, and red dot-dashed curves, respectively.

B. Dark matter as a complex scalar singlet η_1

We now consider the scenario where the complex scalar singlet η_1 plays the role of the DM particle. Compared to the η_2 candidate, η_1 has addition vector interactions because it carries $\mathcal{Y} = -\mathcal{R} = -z/3$ and couples through the Z - Z' mixing. These new interactions contribute to both DM pair annihilation and SI DM-nucleon scattering. The thermally averaged annihilation cross section of η_1 can be written as

$$\langle \sigma v_{\text{rel}} \rangle_{\eta_1^* \eta_1} = \langle \sigma v_{\text{rel}} \rangle_{\eta_1^* \eta_1}^{\text{scalar}} + \langle \sigma v_{\text{rel}} \rangle_{\eta_1^* \eta_1}^{\text{vector}}, \quad (99)$$

where the first term comes to scalar interactions similar to those of η_2 , while the second term originates from vector interactions,

$$\langle \sigma v_{\text{rel}} \rangle_{\eta_1^* \eta_1}^{\text{vector}} = \langle \sigma v_{\text{rel}} \rangle_{\eta_1^* \eta_1 \rightarrow f f^c}^{\text{vector}} + \langle \sigma v_{\text{rel}} \rangle_{\eta_1^* \eta_1 \rightarrow W^+ W^-, Z_1 Z_1}^{\text{vector}} + \langle \sigma v_{\text{rel}} \rangle_{\eta_1^* \eta_1 \rightarrow H Z_1}^{\text{vector}}. \quad (100)$$

It is worth noting that the annihilation cross sections of η_1 into ff^c, W^+W^- , and HZ_1 , mediated by gauge bosons $Z_{1,2}$, are velocity suppressed and therefore not valid near s-channel resonances [61]. Additionally, the annihilation cross section of η_1 into Z_1Z_1 can be approximately expressed as [62]

$$\langle\sigma v_{\text{rel}}\rangle_{\eta_1^*\eta_1\rightarrow Z_1Z_1}^{\text{vector}} \simeq \frac{z^4 s_\varepsilon^4 (g_1^2 + g_2^2)^2}{162\pi m_{\eta_1}^2}, \quad (101)$$

which is also strongly suppressed due to the smallness of s_ε .

For the SI DM–nucleon scattering, the effective Lagrangian describing the vector interactions at the quark level is written as

$$\mathcal{L}_{\eta_1\text{-quark}}^{\text{eff, vector}} = C_{\eta_1 q}^V (\eta_1^* i \not{\partial}_\mu \eta_1) \bar{q} \gamma^\mu q = -\frac{g}{2c_W} \frac{z\sqrt{g_1^2 + g_2^2}}{3} \left(\frac{g_V^{Z_1}(q)s_\varepsilon}{m_{Z_1}^2} - \frac{g_V^{Z_2}(q)c_\varepsilon}{m_{Z_2}^2} \right) (\eta_1^* i \not{\partial}_\mu \eta_1) \bar{q} \gamma^\mu q. \quad (102)$$

At the nucleon level, the corresponding effective interaction takes the form

$$\mathcal{L}_{\eta_1\text{-nucleon}}^{\text{eff, vector}} = C_{\eta_1 N}^V (\eta_1^* i \not{\partial}_\mu \eta_1) \bar{N} \gamma^\mu N, \quad (103)$$

where $C_{\eta_1 N}^V$ denotes the vector-current effective couplings to nucleons. They are given by $C_{\eta_1 p}^V = 2C_{\eta_1 u}^V + C_{\eta_1 d}^V$ and $C_{\eta_1 n}^V = C_{\eta_1 u}^V + 2C_{\eta_1 d}^V$. Hence, the total effective couplings of η_1 and η_1^* to nucleons can be written as

$$C_{\eta_1(\eta_1^*)p} = C_{\eta_1 p}^S \pm C_{\eta_1 p}^V, \quad C_{\eta_1(\eta_1^*)n} = C_{\eta_1 n}^S \pm C_{\eta_1 n}^V, \quad (104)$$

which differ between proton and neutron, as well as between η_1 and η_1^* . The scalar effective couplings $C_{\eta_1 N}^S$ are similar those of η_2 , i.e., $C_{\eta_1 N}^S = C_{\eta_2 N}|_{m_{\eta_2} \rightarrow m_{\eta_1}, \lambda_{28} \rightarrow \lambda_{24}, \lambda_{29} \rightarrow \lambda_{25}}$. The averaged SI cross section of η_1 and η_1^* scattering off a nucleus \mathbb{A} is then given by

$$\sigma_{\eta_1\text{-}\mathbb{A}}^{\text{SI}} = \frac{\mu_{\mathbb{A}}^2}{2\pi} \{ [ZC_{\eta_1 p} + (A - Z)C_{\eta_1 n}]^2 + [ZC_{\eta_1^* p} + (A - Z)C_{\eta_1^* n}]^2 \}. \quad (105)$$

Accordingly, the SI DM–nucleon scattering cross section is estimated as [63, 64]

$$\sigma_{\eta_1}^{\text{SI}} = \frac{\mu_p^2 C_{\eta_1 p}^2}{2\pi} \frac{\sum_i \rho_i \mu_{\mathbb{A}_i}^2 \{ [Z + (A_i - Z)C_{\eta_1 n}/C_{\eta_1 p}]^2 + [ZC_{\eta_1^* p}/C_{\eta_1 p} + (A_i - Z)C_{\eta_1^* n}/C_{\eta_1 p}]^2 \}}{\sum_i \rho_i \mu_{\mathbb{A}_i}^2 A_i^2}, \quad (106)$$

where the nuclear target consists off isotopes A_i with fractional abundance ρ_i (in percent). For example, the natural xenon isotopes have $A_i(\rho_i) = \{128(1.9), 129(26), 130(4.1), 131(21), 132(27), 134(10), 136(8.9)\}$ for xenon isotopes [63].

In Fig. 8, we display the correlation between the SI DM–nucleon cross section $\sigma_{\eta_1}^{\text{SI}}$ and the DM mass m_{η_1} , corresponding to the parameter space that yields the correct DM relic abundance, $\Omega_{\eta_1} h^2 \simeq 0.1 \text{ pb}/\langle\sigma v_{\text{rel}}\rangle_{\eta_1^*\eta_1} \simeq 0.12$, as measured by the Planck experiment [4]. The numerical analysis is carried out with the following representative input parameters: $\lambda_{24} = \lambda_{25} = \lambda_3 = \lambda_4 = \lambda' = 0.1$, $g_1 = g_2 = \sqrt{2}g_Y$, $v_2 = 0.52 \text{ GeV}$, $\Lambda_1 = \Lambda_2 = 10 \text{ TeV}$, $m_{\phi^0} = 2.5 \text{ TeV}$, and $-\mu_0^2 = (0.4\text{--}10) \times 10^4 \text{ GeV}^2$, with $Z = 54$ and the isotopic composition (A_i, ρ_i) corresponding to natural xenon. Two viable mass regions for η_1 are identified: $m_{\eta_1} \simeq 592.208 \text{ GeV}$ for $-\mu_0^2 \simeq (1.33\text{--}4.26) \times 10^4 \text{ GeV}^2$ (left panel), and $m_{\eta_1} \simeq (1.03\text{--}2.50) \text{ TeV}$ for $-\mu_0^2 \simeq (0.89\text{--}5.28) \times 10^4 \text{ GeV}^2$ (right panel). These results are qualitatively similar to those obtained for the η_2 candidate. However, the projected sensitivities of upcoming direct-detection experiments—XENONnT/LZ [57, 58], PandaX-xT [59], and DARWIN [60]—are expected to exclude part, or even all, of the parameter space identified above. To retain viable regions consistent with these future limits, smaller values of the relevant couplings must be considered.

C. Comments on the ϕ^0 scalar doublet dark matter scenario

Since ϕ is an $SU(2)_L$ doublet with $\mathcal{Y} = 1/2 - z/3$ and $\mathcal{R} = z/3$, the real and imaginary components of ϕ^0 couple to the SM Z boson through the interaction $\frac{ig}{2c_W}(S_5 \partial^\mu A_5 - \partial^\mu S_5 A_5)Z_\mu$. If S_5 and A_5 are degenerate in mass, as assumed in this work, this coupling induces a sizable contribution to the SI direct-detection cross section, implying that ϕ^0 cannot serve as a viable DM candidate [65, 66]. Nevertheless, we note that S_5 and A_5 need not be exactly degenerate, as their mixings with other scalar states via the mass matrices $\mathcal{M}_{S,A}^2$ in Eqs. (B9) and (B11) can lift the degeneracy. Assuming a mass splitting between S_5 and A_5 larger than a few hundreds of keV, either S_5 or A_5 could act as a viable DM candidate, provided it is the lightest among the P_D -odd fields [67, 68].

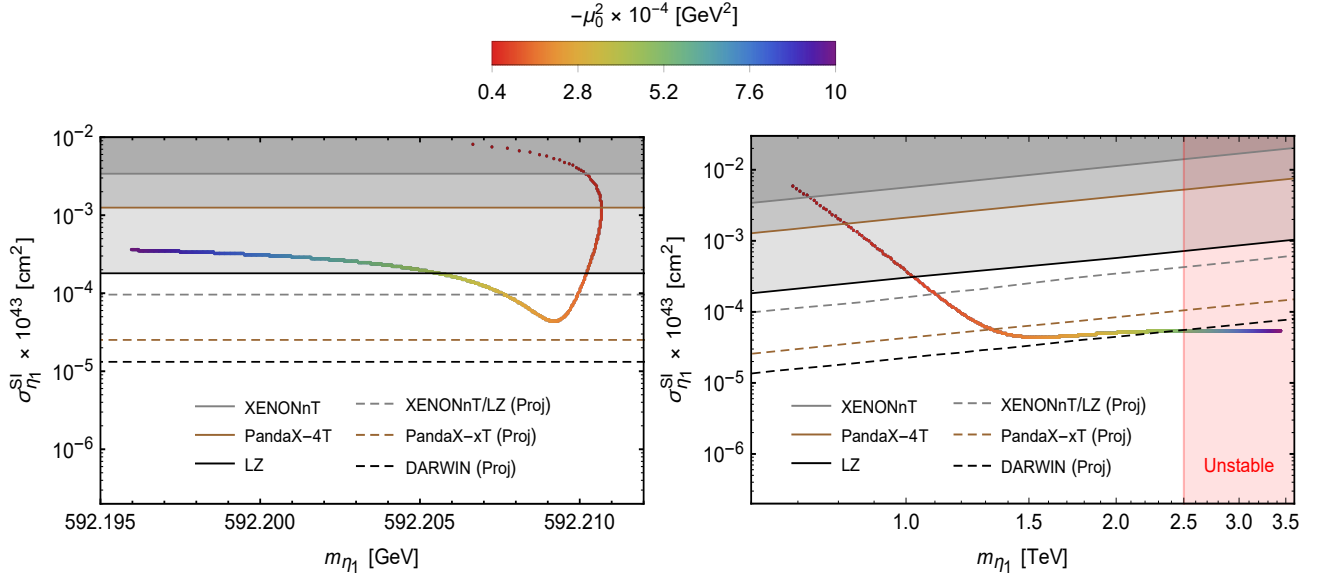


FIG. 8: The same as Fig. 7, except that the results correspond to the DM candidate η_1 .

VI. CONCLUSIONS

In this work, we have proposed a novel extension of the SM based on the flipping principle, enlarging the electroweak gauge symmetry with a double right-handed Abelian structure. This framework leads to a chiral charge assignment, where only the right-handed sector carries nontrivial charges, and provides a unified, anomaly-free construction motivated by left-right symmetric theories and grand unified embeddings. The model offers a natural explanation for the observed SM fermion mass hierarchy. Third-generation of SM charged fermions acquire tree-level masses via Yukawa interactions with the SM Higgs doublet, while the lighter first- and second-generation masses are radiatively generated at one loop level. This radiative mechanism is mediated by a second scalar doublet, which develops a tiny VEV that is itself generated at one-loop level. For neutrinos, masses arise from a combination of a tree-level type-I and a two-loop radiative seesaw mechanism. A key result is that this structure naturally reproduces the observed neutrino mass hierarchy: the atmospheric mass-squared difference originates at tree level, whereas the solar neutrino mass squared splitting emerges at two-loop level. A residual parity symmetry, which survives spontaneous symmetry breaking, stabilizes the lightest parity-odd scalar, providing a viable DM candidate consistent with the experimental value of DM relic abundance and direct detection constraints. Furthermore, this discrete symmetry enforces the radiative nature of the seesaw mechanisms that generate the masses of the first and second generation of SM charged fermions as well as the solar neutrino mass squared splitting. We have examined the phenomenological implications under constraints arising from electroweak precision data, flavor-changing neutral currents, and collider searches. The model predicts new neutral gauge bosons whose signatures are testable at current and future experiments, making the framework both predictive and experimentally accessible.

ACKNOWLEDGEMENT

AECH is supported by ANID-Chile FONDECYT 1241855, ANID – Millennium Science Initiative Program *ICN2019_044*, ANID CCTVal CIA250027 and ICTP through the Associates Programme (2026-2031). N.T.Duy was funded by the Vietnam Academy of Science and Technology, Grant No.CBCLCA.03/25-27.

Appendix A: Scalar potential

The scalar potential of our model can be decomposed as $V = V_1 + V_2 + V_3$, where

$$\begin{aligned} V_1 &= \mu_1^2 \Phi_1^\dagger \Phi_1 + \mu_2^2 \Phi_2^\dagger \Phi_2 + \lambda_1 (\Phi_1^\dagger \Phi_1)^2 + \lambda_2 (\Phi_2^\dagger \Phi_2)^2 + \lambda_3 (\Phi_1^\dagger \Phi_1)(\Phi_2^\dagger \Phi_2) + \lambda_4 (\Phi_1^\dagger \Phi_2)(\Phi_2^\dagger \Phi_1) \\ &\quad + \mu_3^2 \chi_1^* \chi_1 + \mu_4^2 \chi_2^* \chi_2 + \lambda_5 (\chi_1^* \chi_1)^2 + \lambda_6 (\chi_2^* \chi_2)^2 + \lambda_7 (\chi_1^* \chi_1)(\chi_2^* \chi_2) \\ &\quad + \chi_1^* \chi_1 (\lambda_8 \Phi_1^\dagger \Phi_1 + \lambda_9 \Phi_2^\dagger \Phi_2) + \chi_2^* \chi_2 (\lambda_{10} \Phi_1^\dagger \Phi_1 + \lambda_{11} \Phi_2^\dagger \Phi_2), \end{aligned} \quad (\text{A1})$$

$$\begin{aligned} V_2 &= \mu_5^2 \phi^\dagger \phi + \mu_6^2 \eta_1^* \eta_1 + \mu_7^2 \eta_2^* \eta_2 + \lambda_{12} (\phi^\dagger \phi)^2 + \lambda_{13} (\eta_1^* \eta_1)^2 + \lambda_{14} (\eta_2^* \eta_2)^2 + \phi^\dagger \phi (\lambda_{15} \eta_1^* \eta_1 + \lambda_{16} \eta_2^* \eta_2) \\ &\quad + \lambda_{17} (\eta_1^* \eta_1)(\eta_2^* \eta_2) + \phi^\dagger \phi (\lambda_{18} \Phi_1^\dagger \Phi_1 + \lambda_{19} \Phi_2^\dagger \Phi_2 + \lambda_{20} \chi_1^* \chi_1 + \lambda_{21} \chi_2^* \chi_2) + \lambda_{22} (\Phi_1^\dagger \phi)(\phi^\dagger \Phi_1) \\ &\quad + \lambda_{23} (\Phi_2^\dagger \phi)(\phi^\dagger \Phi_2) + \eta_1^* \eta_1 (\lambda_{24} \Phi_1^\dagger \Phi_1 + \lambda_{25} \Phi_2^\dagger \Phi_2 + \lambda_{26} \chi_1^* \chi_1 + \lambda_{27} \chi_2^* \chi_2) \\ &\quad + \eta_2^* \eta_2 (\lambda_{28} \Phi_1^\dagger \Phi_1 + \lambda_{29} \Phi_2^\dagger \Phi_2 + \lambda_{30} \chi_1^* \chi_1 + \lambda_{31} \chi_2^* \chi_2) + \mu (\chi_2 \eta_1^* \eta_2 + \text{H.c.}) \\ &\quad + \lambda [(\Phi_1^\dagger \phi) \chi_2^* \eta_2 + \text{H.c.}] + \lambda' [(\Phi_2^\dagger \phi) \chi_2 \eta_1 + \text{H.c.}], \end{aligned} \quad (\text{A2})$$

$$\begin{aligned} V_3 &= \mu_8^2 \chi_3^* \chi_3 + \lambda_{32} (\chi_3^* \chi_3)^2 + \chi_3^* \chi_3 (\lambda_{33} \Phi_1^\dagger \Phi_1 + \lambda_{34} \Phi_2^\dagger \Phi_2 + \lambda_{35} \chi_1^* \chi_1 + \lambda_{36} \chi_2^* \chi_2) \\ &\quad + \chi_3^* \chi_3 (\lambda_{37} \phi^\dagger \phi + \lambda_{38} \eta_1^* \eta_1 + \lambda_{39} \eta_2^* \eta_2). \end{aligned} \quad (\text{A3})$$

Above, the parameters μ 's have mass dimension, while the λ 's are dimensionless. Without loss of generality, all of them are taken to be real. To begin with, we impose the conditions $\mu_8^2 < 0$ and $\lambda_{32} > 0$, and assume a hierarchy $|\mu_8| \gg |\mu_{1,2,\dots,7}|$ such that the scalar field χ_3 is effectively decoupled from the low-energy dynamics. Under these conditions, χ_3 acquires a large VEV from the potential term V_3 , approximately given by $\Lambda_3^2 \simeq -\mu_8^2/\lambda_{32}$, which spontaneously breaks the $U(1)_R$ symmetry down to a residual parity P_R .

At energy scales below Λ_3 , integrating out the heavy field χ_3 , the effective scalar potential is approximated by $V_{\text{eff}} \simeq V_1 + V_2$. Furthermore, we impose the following conditions:

$$\mu_{1,3,4}^2 < 0, \quad \mu_{2,5,6,7}^2 > 0, \quad \lambda_{1,2,5,6,12,13,14} > 0, \quad |\mu_{3,4}| \gg |\mu_{1,2}|, \quad (\text{A4})$$

to ensure that the scalar fields $\chi_{1,2}$ and Φ_1 develop nonzero VEVs, denoted as $\Lambda_{1,2}$ and v_1 , respectively, with a hierarchy $\Lambda_{1,2} \gg v_1$. In contrast, the scalars ϕ and $\eta_{1,2}$ do not acquire VEVs, which helps maintain the residual parity symmetry. These conditions also imply that the VEV of Φ_2 vanishes at tree level, $\langle \Phi_2 \rangle = v_2/\sqrt{2} = 0$.

However, after the spontaneous breaking of the $U(1)_R \otimes U(1)_R$ symmetry, a nonzero VEV of Φ_2 is radiatively induced at the one-loop level. At energy scales below $\Lambda_{1,2}$, the effective potential involving the two scalar doublets Φ_1 and Φ_2 takes the form

$$\begin{aligned} V(\Phi_1, \Phi_2) &= \mu_1^2 \Phi_1^\dagger \Phi_1 + \mu_2^2 \Phi_2^\dagger \Phi_2 + \lambda_1 (\Phi_1^\dagger \Phi_1)^2 + \lambda_2 (\Phi_2^\dagger \Phi_2)^2 + \lambda_3 (\Phi_1^\dagger \Phi_1)(\Phi_2^\dagger \Phi_2) \\ &\quad + \lambda_4 (\Phi_1^\dagger \Phi_2)(\Phi_2^\dagger \Phi_1) + (\mu_0^2 \Phi_1^\dagger \Phi_2 + \text{H.c.}), \end{aligned} \quad (\text{A5})$$

where the effective coupling μ_0^2 arises from the one-loop diagram shown in Fig. 9, and is given by

$$\mu_0^2 = -\frac{\lambda \lambda' \mu \Lambda_2^3}{16\sqrt{2}\pi^2} \frac{m_{\eta_1}^2 m_{\eta_2}^2 \ln \frac{m_{\eta_1}}{m_{\eta_2}} + m_{\eta_2}^2 m_\phi^2 \ln \frac{m_{\eta_2}}{m_\phi} + m_\phi^2 m_{\eta_1}^2 \ln \frac{m_\phi}{m_{\eta_1}}}{(m_{\eta_1}^2 - m_{\eta_2}^2)(m_{\eta_2}^2 - m_\phi^2)(m_{\eta_1}^2 - m_\phi^2)}. \quad (\text{A6})$$

The masses of the scalar fields entering the loop are given by

$$m_\phi^2 = \mu_5^2 + \frac{1}{2} [(\lambda_{18} + \lambda_{22}) v_1^2 + \lambda_{20} \Lambda_1^2 + \lambda_{21} \Lambda_2^2], \quad (\text{A7})$$

$$m_{\eta_1}^2 = \mu_6^2 + \frac{1}{2} (\lambda_{24} v_1^2 + \lambda_{26} \Lambda_1^2 + \lambda_{27} \Lambda_2^2), \quad (\text{A8})$$

$$m_{\eta_2}^2 = \mu_7^2 + \frac{1}{2} (\lambda_{28} v_1^2 + \lambda_{30} \Lambda_1^2 + \lambda_{31} \Lambda_2^2). \quad (\text{A9})$$

Assuming $\mu_0^2 < 0$ and $\sqrt{-\mu_0^2} \sim v_1$, the VEV of Φ_2 is approximately given by

$$v_2 \simeq -\frac{2v_1 \mu_0^2}{2\mu_2^2 + (\lambda_3 + \lambda_4) v_1^2 + \lambda_9 \Lambda_1^2 + \lambda_{11} \Lambda_2^2}, \quad (\text{A10})$$

under the assumption that $v_2 \ll v_1$. As a representative example, taking $\lambda\lambda' \sim \mathcal{O}(0.1)$, $\mu \sim \mathcal{O}(10)$ GeV, $\Lambda_2 \sim \mathcal{O}(10^4)$ GeV, and $m_\phi \sim m_{\eta_1} \sim m_{\eta_2} \sim \mathcal{O}(10^3)$ GeV, we have $-\mu_0^2 \sim \mathcal{O}(10^4)$ GeV². Also, for $v_1 \sim \mathcal{O}(10^2)$ GeV, $\mu_2 \ll v_1$, $\lambda_3 \sim \lambda_4 \sim \mathcal{O}(0.1)$, $\Lambda_1 \sim \Lambda_2 \sim \mathcal{O}(10^4)$ GeV, and $\lambda_9 \sim \lambda_{11} \sim \mathcal{O}(10^{-2})$, the resulting value $v_2 \sim 1$ GeV is sufficient to generate the charm quark mass with an associated Yukawa coupling of order one. Finally, the VEVs $v_{1,2}$ break the electroweak symmetry $SU(2)_L \otimes U(1)_Y$ down to $U(1)_Q$, and simultaneously shift the residual parity $P_R = (-1)^{2R}$ to a new conserved parity $P_D = (-1)^{2D}$.

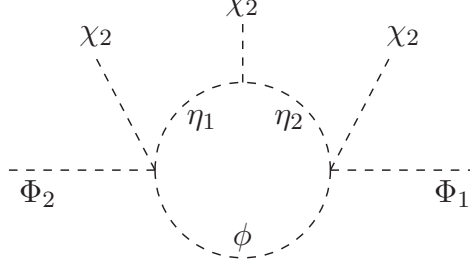


FIG. 9: One-loop diagram generating the $\mu_0^2 \Phi_1^\dagger \Phi_2$ term in the scalar potential.

Appendix B: Mass matrix in scalar sector

To determine the mass matrices in the scalar sector, we expand the scalar fields around their VEVs, namely:

$$\Phi_1^0 = \frac{1}{\sqrt{2}}(v_1 + S_1 + iA_1), \quad \Phi_2^0 = \frac{1}{\sqrt{2}}(v_2 + S_2 + iA_2), \quad (B1)$$

$$\chi_1 = \frac{1}{\sqrt{2}}(\Lambda_1 + S_3 + iA_3), \quad \chi_2 = \frac{1}{\sqrt{2}}(\Lambda_2 + S_4 + iA_4), \quad (B2)$$

$$\phi^0 = \frac{1}{\sqrt{2}}(S_5 + iA_5), \quad \eta_1 = \frac{1}{\sqrt{2}}(S_6 + iA_6), \quad \eta_2 = \frac{1}{\sqrt{2}}(S_7 + iA_7). \quad (B3)$$

Substituting the expanded scalar fields into the effective potential $V_{\text{eff}} \simeq V_1 + V_2 + (\mu_0^2 \Phi_1^\dagger \Phi_2 + \text{H.c.})$, we obtain the conditions for the potential minimum as follows:

$$2\mu_0^2 v_2 + 2\mu_1^2 v_1 + 2\lambda_1 v_1^3 + (\lambda_3 + \lambda_4) v_1 v_2^2 + \lambda_8 \Lambda_1^2 v_1 + \lambda_{10} \Lambda_2^2 v_1 = 0, \quad (B4)$$

$$2\mu_0^2 v_1 + 2\mu_2^2 v_2 + 2\lambda_2 v_2^3 + (\lambda_3 + \lambda_4) v_1^2 v_2 + \lambda_9 \Lambda_1^2 v_2 + \lambda_{11} \Lambda_2^2 v_2 = 0, \quad (B5)$$

$$2\mu_3^2 + 2\lambda_5 \Lambda_1^2 + \lambda_7 \Lambda_2^2 + \lambda_8 v_1^2 + \lambda_9 v_2^2 = 0, \quad (B6)$$

$$2\mu_4^2 + 2\lambda_6 \Lambda_2^2 + \lambda_7 \Lambda_1^2 + \lambda_{10} v_1^2 + \lambda_{11} v_2^2 = 0. \quad (B7)$$

Hence, we determine the mass matrices of scalar bosons. For the CP-even scalar bosons, we obtain two separate mass matrices,

$$M_S^2 = \begin{pmatrix} 2\lambda_1 v_1^2 - \frac{\mu_0^2 v_2}{v_1} & (\lambda_3 + \lambda_4) v_1 v_2 + \mu_0^2 & \lambda_8 \Lambda_1 v_1 & \lambda_{10} \Lambda_2 v_1 \\ (\lambda_3 + \lambda_4) v_1 v_2 + \mu_0^2 & 2\lambda_2 v_2^2 - \frac{\mu_0^2 v_1}{v_2} & \lambda_9 \Lambda_1 v_2 & \lambda_{11} \Lambda_2 v_2 \\ \lambda_8 \Lambda_1 v_1 & \lambda_9 \Lambda_1 v_2 & 2\lambda_5 \Lambda_1^2 & \lambda_7 \Lambda_1 \Lambda_2 \\ \lambda_{10} \Lambda_2 v_1 & \lambda_{11} \Lambda_2 v_2 & \lambda_7 \Lambda_1 \Lambda_2 & 2\lambda_6 \Lambda_2^2 \end{pmatrix}, \quad (B8)$$

and

$$\mathcal{M}_S^2 = \begin{pmatrix} m_\phi^2 + \frac{\lambda_{19} + \lambda_{23}}{2} v_2^2 & \frac{\lambda' \Lambda_2 v_2}{2} & \frac{\lambda \Lambda_2 v_1}{2} \\ \frac{\lambda' \Lambda_2 v_2}{2} & m_{\eta_1}^2 + \frac{\lambda_{25}}{2} v_2^2 & \frac{\mu \Lambda_2}{\sqrt{2}} \\ \frac{\lambda \Lambda_2 v_1}{2} & \frac{\mu \Lambda_2}{\sqrt{2}} & m_{\eta_2}^2 + \frac{\lambda_{29}}{2} v_2^2 \end{pmatrix}, \quad (B9)$$

in the bases (S_1, S_2, S_3, S_4) and (S_5, S_6, S_7) , respectively. For the CP-odd scalar bosons, we similarly find two mass matrices,

$$M_A^2 = \begin{pmatrix} -\frac{\mu_0^2 v_2}{v_1} & \mu_0^2 \\ \mu_0^2 & -\frac{\mu_0^2 v_1}{v_2} \end{pmatrix}, \quad (\text{B10})$$

and

$$\mathcal{M}_A^2 = \begin{pmatrix} m_\phi^2 + \frac{\lambda_{19} + \lambda_{23}}{2} v_2^2 & -\frac{\lambda' \Lambda_2 v_2}{2} & -\frac{\lambda \Lambda_2 v_1}{2} \\ -\frac{\lambda' \Lambda_2 v_2}{2} & m_{\eta_1}^2 + \frac{\lambda_{25}}{2} v_2^2 & \frac{\mu \Lambda_2}{\sqrt{2}} \\ -\frac{\lambda \Lambda_2 v_1}{2} & \frac{\mu \Lambda_2}{\sqrt{2}} & m_{\eta_2}^2 + \frac{\lambda_{29}}{2} v_2^2 \end{pmatrix}, \quad (\text{B11})$$

in the bases (A_1, A_2) and (A_5, A_6, A_7) , respectively. Finally, for the charged scalar bosons, the mass matrix in the basis $(\Phi_1^\pm, \Phi_2^\pm, \phi^\pm)$ takes the form

$$M_C^2 = \begin{pmatrix} -\frac{(\lambda_4 v_1 v_2 + 2\mu_0^2)v_2}{2v_1} & \frac{\lambda_4 v_1 v_2}{2} + \mu_0^2 & 0 \\ \frac{\lambda_4 v_1 v_2}{2} + \mu_0^2 & -\frac{(\lambda_4 v_1 v_2 + 2\mu_0^2)v_1}{2v_2} & 0 \\ 0 & 0 & m_\phi^2 + \frac{1}{2}(\lambda_{19} v_2^2 - \lambda_{22} v_1^2) \end{pmatrix}. \quad (\text{B12})$$

[1] PARTICLE DATA GROUP collaboration, *Review of particle physics*, *Phys. Rev. D* **110** (2024) 030001.

[2] T. Kajita, *Nobel Lecture: Discovery of atmospheric neutrino oscillations*, *Rev. Mod. Phys.* **88** (2016) 030501.

[3] A. B. McDonald, *Nobel Lecture: The Sudbury Neutrino Observatory: Observation of flavor change for solar neutrinos*, *Rev. Mod. Phys.* **88** (2016) 030502.

[4] PLANCK collaboration, *Planck 2018 results. VI. Cosmological parameters*, *Astron. Astrophys.* **641** (2020) A6 [1807.06209].

[5] R. P. Feynman and M. Gell-Mann, *Theory of Fermi interaction*, *Phys. Rev.* **109** (1958) 193.

[6] E. C. G. Sudarshan and R. e. Marshak, *Chirality invariance and the universal Fermi interaction*, *Phys. Rev.* **109** (1958) 1860.

[7] J. J. Sakurai, *MASS REVERSAL AND WEAK INTERACTIONS*, *Nuovo Cim.* **7** (1958) 649.

[8] S. L. Glashow, *Partial Symmetries of Weak Interactions*, *Nucl. Phys.* **22** (1961) 579.

[9] S. Weinberg, *A Model of Leptons*, *Phys. Rev. Lett.* **19** (1967) 1264.

[10] P. Van Dong, *Flipping principle for neutrino mass and dark matter*, *Phys. Rev. D* **102** (2020) 011701 [2003.13276].

[11] D. Van Loi, C. H. Nam, N. H. Tan and P. Van Dong, *Dark charge versus electric charge*, *Phys. Rev. D* **105** (2022) 075012 [2004.06005].

[12] D. Van Loi, N. M. Duc and P. V. Dong, *Dequantization of electric charge: Probing scenarios of cosmological multi-component dark matter*, *Nucl. Phys. B* **983** (2022) 115924 [2106.12278].

[13] P. Van Dong and D. Van Loi, *Gauge Origin of Double Dark Parity and Implication for Dark Matter*, *Commun. in Phys.* **32** (2022) 101 [2110.01236].

[14] L. M. Krauss, S. Nasri and M. Trodden, *A Model for neutrino masses and dark matter*, *Phys. Rev. D* **67** (2003) 085002 [hep-ph/0210389].

[15] E. Ma, *Verifiable radiative seesaw mechanism of neutrino mass and dark matter*, *Phys. Rev. D* **73** (2006) 077301 [hep-ph/0601225].

[16] L. Lopez Honorez, E. Nezri, J. F. Oliver and M. H. G. Tytgat, *The Inert Doublet Model: An Archetype for Dark Matter*, *JCAP* **02** (2007) 028 [hep-ph/0612275].

[17] N. Okada and O. Seto, *Higgs portal dark matter in the minimal gauged $U(1)_{B-L}$ model*, *Phys. Rev. D* **82** (2010) 023507 [1002.2525].

[18] A. Das, S. Goswami, K. N. Vishnudath and T. Nomura, *Constraining a general $U(1)'$ inverse seesaw model from vacuum stability, dark matter and collider*, *Phys. Rev. D* **101** (2020) 055026 [1905.00201].

[19] C. H. Nam, *Flipped $U(1)$ extended Standard Model and Majorana dark matter*, *Eur. Phys. J. C* **80** (2020) 1114 [2011.11207].

[20] A. Das, S. Gola, S. Mandal and N. Sinha, *Two-component scalar and fermionic dark matter candidates in a generic $U(1)X$ model*, *Phys. Lett. B* **829** (2022) 137117 [2202.01443].

[21] S. K. A., A. Das, G. Lambiase, T. Nomura and Y. Orikasa, *Probing chiral and flavored Z' from cosmic bursts through neutrino interactions*, *Eur. Phys. J. C* **84** (2024) 1224 [2308.14483].

- [22] D. Van Loi, C. H. Nam and P. Van Dong, *Phenomenology of a minimal extension of the standard model with a family-dependent gauge symmetry*, *Phys. Rev. D* **108** (2023) 095018 [2305.04681].
- [23] T. Nomura and H. Okada, *Loop suppressed light fermion masses with $U(1)_R$ gauge symmetry*, *Phys. Rev. D* **96** (2017) 015016 [1704.03382].
- [24] D. Chang and R. N. Mohapatra, *Small and Calculable Dirac Neutrino Mass*, *Phys. Rev. Lett.* **58** (1987) 1600.
- [25] S. Kanemura and H. Sugiyama, *Dark matter and a suppression mechanism for neutrino masses in the Higgs triplet model*, *Phys. Rev. D* **86** (2012) 073006 [1202.5231].
- [26] S. Kanemura, T. Matsui and H. Sugiyama, *Loop Suppression of Dirac Neutrino Mass in the Neutrinophilic Two Higgs Doublet Model*, *Phys. Lett. B* **727** (2013) 151 [1305.4521].
- [27] S. P. Martin, *A Supersymmetry primer*, *Adv. Ser. Direct. High Energy Phys.* **18** (1998) 1 [hep-ph/9709356].
- [28] D. Van Loi and P. Van Dong, *Flavor-dependent $U(1)$ extension inspired by lepton, baryon and color numbers*, *Eur. Phys. J. C* **83** (2023) 1048 [2307.13493].
- [29] E. K. Akhmedov, Z. G. Berezhiani, R. N. Mohapatra and G. Senjanovic, *Planck scale effects on the majoron*, *Phys. Lett. B* **299** (1993) 90 [hep-ph/9209285].
- [30] I. Z. Rothstein, K. S. Babu and D. Seckel, *Planck scale symmetry breaking and majoron physics*, *Nucl. Phys. B* **403** (1993) 725 [hep-ph/9301213].
- [31] A. Dupays, E. Masso, J. Redondo and C. Rizzo, *Light scalars coupled to photons and non-newtonian forces*, *Phys. Rev. Lett.* **98** (2007) 131802 [hep-ph/0610286].
- [32] D. Van Loi, P. Van Dong, N. T. Duy and N. H. Thao, *Questions of flavor physics and neutrino mass from a flipped hypercharge*, *Phys. Rev. D* **109** (2024) 115022 [2312.12836].
- [33] D. Van Loi, N. T. Duy, C. H. Nam and P. Van Dong, *Scoto-seesaw model implied by flavor-dependent Abelian gauge charge*, *Eur. Phys. J. C* **85** (2025) 109 [2409.06393].
- [34] Z.-z. Xing, *Flavor structures of charged fermions and massive neutrinos*, *Phys. Rept.* **854** (2020) 1 [1909.09610].
- [35] I. Esteban, M. C. Gonzalez-Garcia, M. Maltoni, I. Martinez-Soler, J. a. P. Pinheiro and T. Schwetz, *NuFit-6.0: updated global analysis of three-flavor neutrino oscillations*, *JHEP* **12** (2024) 216 [2410.05380].
- [36] ALEPH, DELPHI, L3, OPAL, SLD, LEP ELECTROWEAK WORKING GROUP, SLD ELECTROWEAK GROUP, SLD HEAVY FLAVOUR GROUP collaboration, *Precision electroweak measurements on the Z resonance*, *Phys. Rept.* **427** (2006) 257 [hep-ex/0509008].
- [37] J. Erler, P. Langacker, S. Munir and E. Rojas, *Improved Constraints on Z -prime Bosons from Electroweak Precision Data*, *JHEP* **08** (2009) 017 [0906.2435].
- [38] D. Van Loi, A. E. Cárcamo Hernández, V. Q. Tran and N. T. Duy, *Tri-hypercharge versus tri-darkcharge*, 2506.12873.
- [39] A. J. Buras, F. De Fazio, J. Girrbach and M. V. Carlucci, *The Anatomy of Quark Flavour Observables in 331 Models in the Flavour Precision Era*, *JHEP* **02** (2013) 023 [1211.1237].
- [40] T. Inami and C. S. Lim, *Effects of Superheavy Quarks and Leptons in Low-Energy Weak Processes $k(L) \rightarrow \mu \text{ anti-}\mu$, $K \rightarrow \pi + \text{Neutrino anti-neutrino}$ and $K0 \leftrightarrow \text{anti-}K0$* , *Prog. Theor. Phys.* **65** (1981) 297.
- [41] A. J. Buras, M. Jamin and P. H. Weisz, *Leading and Next-to-leading QCD Corrections to ϵ Parameter and $B^0 - \bar{B}^0$ Mixing in the Presence of a Heavy Top Quark*, *Nucl. Phys. B* **347** (1990) 491.
- [42] J. A. Bagger, K. T. Matchev and R.-J. Zhang, *QCD corrections to flavor changing neutral currents in the supersymmetric standard model*, *Phys. Lett. B* **412** (1997) 77 [hep-ph/9707225].
- [43] A. J. Buras, R. Fleischer, J. Girrbach and R. Knegjens, *Probing New Physics with the $B_s \rightarrow \mu + \mu -$ Time-Dependent Rate*, *JHEP* **07** (2013) 077 [1303.3820].
- [44] M. Czaja and M. Misiak, *Current Status of the Standard Model Prediction for the $B_s \rightarrow \mu^+ \mu^-$ Branching Ratio*, *Symmetry* **16** (2024) 917 [2407.03810].
- [45] LEP, ALEPH, DELPHI, L3, LEP ELECTROWEAK WORKING GROUP, SLD ELECTROWEAK GROUP, SLD HEAVY FLAVOUR GROUP, OPAL collaboration, *A Combination of preliminary electroweak measurements and constraints on the standard model*, hep-ex/0412015.
- [46] M. Carena, A. Daleo, B. A. Dobrescu and T. M. P. Tait, *Z' gauge bosons at the Tevatron*, *Phys. Rev. D* **70** (2004) 093009 [hep-ph/0408098].
- [47] A. Das, P. S. B. Dev, Y. Hosotani and S. Mandal, *Probing the minimal $U(1)X$ model at future electron-positron colliders via fermion pair-production channels*, *Phys. Rev. D* **105** (2022) 115030 [2104.10902].
- [48] ATLAS collaboration, *Search for high-mass dilepton resonances using 139 fb^{-1} of pp collision data collected at $\sqrt{s} = 13 \text{ TeV}$ with the ATLAS detector*, *Phys. Lett. B* **796** (2019) 68 [1903.06248].
- [49] CMS collaboration, *Search for resonant and nonresonant new phenomena in high-mass dilepton final states at $\sqrt{s} = 13 \text{ TeV}$* , *JHEP* **07** (2021) 208 [2103.02708].
- [50] P. Junnarkar and A. Walker-Loud, *Scalar strange content of the nucleon from lattice QCD*, *Phys. Rev. D* **87** (2013) 114510 [1301.1114].

- [51] M. Hoferichter, J. Ruiz de Elvira, B. Kubis and U.-G. Meißner, *High-Precision Determination of the Pion-Nucleon σ Term from Roy-Steiner Equations*, *Phys. Rev. Lett.* **115** (2015) 092301 [[1506.04142](#)].
- [52] G. Jungman, M. Kamionkowski and K. Griest, *Supersymmetric dark matter*, *Phys. Rept.* **267** (1996) 195 [[hep-ph/9506380](#)].
- [53] J. L. Feng, J. Kumar and D. Sanford, *Xenophobic Dark Matter*, *Phys. Rev. D* **88** (2013) 015021 [[1306.2315](#)].
- [54] XENON collaboration, *First Dark Matter Search with Nuclear Recoils from the XENONnT Experiment*, *Phys. Rev. Lett.* **131** (2023) 041003 [[2303.14729](#)].
- [55] PANDAX collaboration, *Dark Matter Search Results from 1.54 Tonne-Year Exposure of PandaX-4T*, *Phys. Rev. Lett.* **134** (2025) 011805 [[2408.00664](#)].
- [56] LZ collaboration, *Dark Matter Search Results from 4.2 Tonne-Years of Exposure of the LUX-ZEPLIN (LZ) Experiment*, *Phys. Rev. Lett.* **135** (2025) 011802 [[2410.17036](#)].
- [57] XENON collaboration, *Projected WIMP sensitivity of the XENONnT dark matter experiment*, *JCAP* **11** (2020) 031 [[2007.08796](#)].
- [58] LZ collaboration, *Projected WIMP sensitivity of the LUX-ZEPLIN dark matter experiment*, *Phys. Rev. D* **101** (2020) 052002 [[1802.06039](#)].
- [59] PANDA-X, PANDAX collaboration, *PandaX-xT—A deep underground multi-ten-tonne liquid xenon observatory*, *Sci. China Phys. Mech. Astron.* **68** (2025) 221011 [[2402.03596](#)].
- [60] DARWIN collaboration, *DARWIN: towards the ultimate dark matter detector*, *JCAP* **11** (2016) 017 [[1606.07001](#)].
- [61] K. Griest and D. Seckel, *Three exceptions in the calculation of relic abundances*, *Phys. Rev. D* **43** (1991) 3191.
- [62] G. Arcadi, M. Dutra, P. Ghosh, M. Lindner, Y. Mambrini, M. Pierre et al., *The waning of the WIMP? A review of models, searches, and constraints*, *Eur. Phys. J. C* **78** (2018) 203 [[1703.07364](#)].
- [63] J. L. Feng, J. Kumar, D. Marfatia and D. Sanford, *Isospin-Violating Dark Matter*, *Phys. Lett. B* **703** (2011) 124 [[1102.4331](#)].
- [64] J. Lao, C. Cai, Z.-H. Yu, Y.-P. Zeng and H.-H. Zhang, *Fermionic and scalar dark matter with hidden U(1) gauge interaction and kinetic mixing*, *Phys. Rev. D* **101** (2020) 095031 [[2003.02516](#)].
- [65] M. Cirelli, N. Fornengo and A. Strumia, *Minimal dark matter*, *Nucl. Phys. B* **753** (2006) 178 [[hep-ph/0512090](#)].
- [66] R. Barbieri, L. J. Hall and V. S. Rychkov, *Improved naturalness with a heavy Higgs: An Alternative road to LHC physics*, *Phys. Rev. D* **74** (2006) 015007 [[hep-ph/0603188](#)].
- [67] E. M. Dolle and S. Su, *The Inert Dark Matter*, *Phys. Rev. D* **80** (2009) 055012 [[0906.1609](#)].
- [68] T. de Boer, R. Busse, A. Kappes, M. Klasen and S. Zeinstra, *Indirect detection constraints on the scotogenic dark matter model*, *JCAP* **08** (2021) 038 [[2105.04899](#)].